NEURAL+SYMBOLIC ACTOR-CRITIC FRAMEWORK FOR INTERPRETABLE REINFORCEMENT LEARNING

Anonymous authors
Paper under double-blind review

ABSTRACT

The integration of neural networks into actor-critic frameworks has been pivotal in advancing the field of reinforcement learning, enabling agents to perform complex tasks with greater efficiency and adaptability. However, neural network-based actor-critic models remain opaque "black boxes," concealing their decision-making processes and hindering their use in critical applications where transparent and explainable reasoning is essential. This work introduces an innovative adaptation of the actor-critic framework that unites neural networks with rule ensembles to tackle key challenges in reinforcement learning. We harness the computational power, scalability, and adaptability of neural networks to model the critic, while integrating a rule ensemble system for the actor, ensuring transparency and interpretability for decision-making. Our study establishes a theoretical foundation for integrating rule ensembles into the Advantage Actor-Critic (A2C) framework. Experimental results from seven classic and complex environments demonstrate that our proposed method matches or exceeds the performance of representative RL models, including symbolic methods, while offering self-interpretability and transparency.

1 INTRODUCTION

Actor-critic reinforcement learning (RL) methods, such as Advantage Actor-Critic (A2C) and Proximal Policy Optimization (PPO), have delivered exceptional performance across diverse RL tasks (Mnih et al., 2016; Schulman et al., 2017), largely due to the use of neural networks to effectively manage complex, high-dimensional state-action spaces. Yet, as actor-critic RL models expand to broader real-world domains, such as healthcare, finance, and law, interpretability becomes essential for ensuring trust, transparency, and regulation compliance in decision-making. By revealing how actions are chosen or why specific decisions are made, interpretability supports debugging, model improvement, and the ability to explain automated decisions in line with legal and ethical standards.

Despite the effectiveness of neural network-based actor-critic models, their opaque nature and lack of transparency can limit their use in sensitive or critical applications where comprehending the rationale behind each decision is crucial (Benítez et al., 1997; Castelvecchi, 2016). Symbolic models, e.g., expert systems, decision trees, and rule-based systems, rely on clear, well-defined rules and logic to make decisions, allowing for easier tracing of how conclusions are reached (Ernst et al., 2005; Gupta et al., 2015a; Tao et al., 2018; Bastani et al., 2018; Illanes et al., 2020). These methods use symbols (which can represent objects, properties, or relationships) and logic to process and reason about data, making the decision-making process transparent and understandable.

However, substituting neural network-based models with symbolic models in reinforcement learning tasks can be challenging. (i) While symbolic methods are highly valued for their interpretability and transparency, current implementations in reinforcement learning typically rely on predefined knowledge or pre-trained models (Garcez et al., 2018; Lyu et al., 2019). (ii) These symbolic methods can face challenges in managing the complexity and ambiguity that non-symbolic approaches, such as neural networks, are often better equipped to handle (Illanes et al., 2020; Landajuela et al., 2021).

To tackle the above challenges, we propose a new "**N**eural plus **S**ymbolic" framework for **A**ctor-**C**ritic models, namely **NSAC**, as shown in Figure 1. NSAC integrates the strengths of both neural networks and symbolic rule-based systems. Specifically, the neural critic leverages powerful function approximation capabilities to estimate the value of states and state-action pairs effectively. Meanwhile,

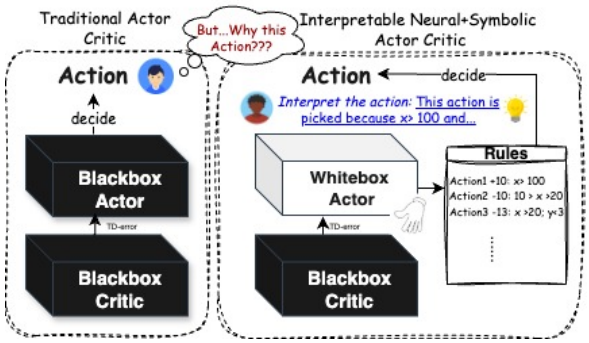

Figure 1: Comparative illustration of Neural+Symbolic Actor-Critic (NSAC) and classic Actor-Critic methods.

the actor component is designed using a rule-based approach, providing intrinsic interpretability by following explicit, predefined rules that govern its decision-making process. This framework allows for an analysis of how particular features or rules influence decisions, offering a level of explainability absent in black-box models. Our theoretical analysis proves that NSAC converges to a local optimum. Through empirical experiments, our proposed NSAC demonstrates performance levels that match those of widely-used reinforcement learning algorithms, such as DQN (Mnih, 2013), PPO (Schulman et al., 2017), Rainbow (Hessel et al., 2018), SDSAC (Kong et al., 2021), SACBBF (Zhang et al., 2024), and A2C (Mnih et al., 2016). By integrating the adaptability and generalization capabilities of neural networks with the transparency of rule-based decision-making, our model provides a balanced solution that retains high performance while enabling interpretable and trustworthy decision-making processes. It is worth noting that, our work belongs to the broader neural-symbolic family, but differs from compile-logic approaches. NSAC uniquely couples a data-driven neural critic with a rule-based symbolic actor, enabling both statistical learning and explicit reasoning within an actor–critic loop. This work makes three main contributions:

- We propose a novel actor–critic architecture that combines a neural critic for accurate value estimation with a symbolic, rule-based actor that delivers intrinsic interpretability.
- We provide a formal proof of convergence and demonstrate that our rule-based policy satisfies the established interpretability criteria of simulatability, modularity, and low complexity (Murdoch et al., 2019).
- We empirically demonstrate that NSAC matches state-of-the-art RL methods on classic control and energy-system tasks, while uniquely preserving transparency and trustworthiness.

2 Related Work

Interpretability has become increasingly important in RL and motivated symbolic approaches that provide transparent reasoning while retaining RL's adaptive capabilities. Existing approaches can be categorized based on their interpretability characteristics, knowledge requirements, and learning paradigms, each with distinct limitations. Tree-based policies represent a widely studied approach to interpretable RL. Native tree methods (Ding et al., 2020; Ernst et al., 2005; Gupta et al., 2015a; Roth et al., 2019; Tao et al., 2018) learn decision trees directly from environmental interactions, often achieving strong performance on small to medium-scale problems but facing scalability challenges where large trees become difficult to interpret. Distillation-based tree methods (Bastani et al., 2018; Coppens et al., 2019; Gupta et al., 2015b; Liu et al., 2019) extract tree policies from pre-trained neural networks, but face a size versus fidelity trade-off. Their differentiable variants (Silva et al., 2020) and specialized architectures (Ding et al., 2020; Liu et al., 2019) attempt to address these limitations but may produce mathematical notations and complex tree structures that remain difficult for humans to interpret. Symbolic RL with predefined knowledge leverages domain expertise to guide policy learning. These methods (Garcez et al., 2018; Illanes et al., 2020; Lyu et al., 2019) can maintain interpretability through symbolic rules, modules, or plans, and may achieve strong performance when domain priors are well-specified. However, they require substantial predefined knowledge, making them sensitive to domain assumptions and limiting their applicability to new domains where such expertise may not be available. To remove this dependency, symbolic policies learn from neural teachers or direct search to discover symbolic representations, such as neural-guided symbolic policy discovery (Landajuela et al., 2021), genetic programming for symbolic expressions (Hein et al., 2018), and program synthesis approaches (Wu et al., 2020; Qiu & Zhu, 2022). While these methods avoid predefined knowledge, they often yield complex mathematical expressions involving trigonometric functions, logarithms, or program syntax that are challenging for humans to simulate and interpret (Murdoch et al., 2019). Recent work like SYMPOL (Marton et al., 2024) optimizes

tree policies directly but suffers performance degradation in complex domain. Post-hoc approaches additionally may suffer from approximation errors inherited from neural teachers.

As discussed, most previous methods either require a certain amount of predefined knowledge, which influences the search space or establishes the programmatic rules, or they are post-hoc solutions that learn from a pre-trained model rather than directly from the environment, potentially distorting the learning objectives. In contrast, our method effectively integrates a neural network-based critic with a symbolic, rule-based, interpretable actor by learning directly through environmental interactions without requiring predefined knowledge. Specifically, we address the tree scalability problem by using additive rule ensembles rather than hierarchical structures, where each rule contributes equally to the decision-making process. We employ Orthogonal Gradient Boosting (OGB) (Yang et al., 2024) to discover rule conditions automatically, requiring only basic feature comparisons rather than domain-specific knowledge. Our rule-based actor is trained directly via policy gradients on environmental rewards, ensuring the symbolic representation accurately reflects true decision-making process rather than approximating a black-box teacher. Our approach achieves interpretability through symbolic rules while learning directly from the environment, addressing both the knowledge requirements and post-hoc limitations of existing methods. Post-hoc explainers are only approximations: they often flag correlates, not causes. SHAP (Lundberg & Lee, 2017), for example, mark a feature as "important" while the model flips under tiny perturbations. Worse, black-box models can even be trained to emit persuasive but misleading rationales (Rudin, 2019). Because these explanations are extrinsic, they guarantee neither consistency, fidelity, nor out-of-distribution robustness.

3 PRELIMINARIES

3.1 ADVANTAGE ACTOR-CRITIC REINFORCEMENT LEARNING

The A2C algorithm represents a synergy of two foundational approaches in reinforcement learning: the actor-critic method and the advantage function estimation. In the actor-critic framework, the critic in the A2C framework estimates the value function $V(s)$, which represents the expected return from a state s. The critic is updated by minimizing its loss function, typically the mean squared error between the estimated value and the computed target value. The target value is derived from the rewards obtained and the discounted values of subsequent states: $L_V(\phi) = \mathbb{E}\left[\left(R_t + \gamma V(s_{t+1}) - V_\phi(s_t)\right)^2\right]$, where R_t is the reward received after taking action a_t in state s_t at t, γ is the discount factor, $V_\phi(s_{t+1})$ is the value estimate for the next state at $t+1$, and ϕ are the parameters of the critic network. The actor updates the policy by adjusting parameters θ in the direction suggested by the critic's evaluations. The update is guided by the gradient of the policy's performance, estimated using the advantage function: $\nabla_\theta L(\theta) = \mathbb{E}\left[\nabla_\theta \log \pi_\theta(a_t|s_t)\mathcal{A}_t\right]$, where $\mathcal{A}_t = R_t + \gamma V(s_{t+1}) - V(s_t)$ is the advantage at time t, indicating how much better (or worse) the action a_t is than the policy's average at state s_t. Through these updates, the actor learns to choose actions yielding higher returns than predicted by the critic, while the critic learns to make more accurate predictions about expected returns, forming a feedback loop that enhances both policy and value estimation in the A2C framework.

3.2 ADDITIVE RULE ENSEMBLES

Additive rule ensembles are a class of probabilistic models (Friedman & Popescu, 2008) that estimate the expected value of a target variable $Y \in \mathbb{R}$ given an input vector $\mathbf{X} \in \mathbb{R}^d$, which is expressed as $\mathbb{E}[Y \mid \mathbf{X} = \boldsymbol{x}] = \mu(f(\boldsymbol{x}))$, where, $\boldsymbol{x}$ is an instance of $\mathbf{X}$, $\mu : \mathbb{R} \to \mathbb{R}$ is an inverse link function mapping $f(\boldsymbol{x})$ to the target variable Y, and $f : \mathbb{R}^d \to \mathbb{R}$ is a linear combination of k Boolean query functions:

$$f(\boldsymbol{x}) = \sum_{i=1}^{k} w_i q_i(\boldsymbol{x}) = \sum_{i=1}^{k} w_i \prod_{j=1}^{c_i} p_{i,j}(\boldsymbol{x}). \tag{1}$$

In equation 1, w_i $(0 \leq i \leq k)$ is the weight of the i-th Boolean query function $q_i : \mathbb{R}^d \to \{0, 1\}$, and q_i is a conjunction or product of c_i Boolean propositions, where $p_{i,j} \in \left\{\mathbb{I}\left(sx^{(j)} \leq sx_l^{(j)}\right) : j \in [d], l \in [n], s \in \{\pm 1\}\right\}$ is a threshold function ($[x] = \{1, \ldots, x\}$ is the index set). Each term $w_i q_i(\boldsymbol{x})$ in equation 1 can be represented as an 'IF…THEN …' rule, where the query q_i defines the condition of the rule, and the weight w_i is the rule's consequent.

Boosting is an iterative approach for learning additive models (Schapire, 1990; Friedman, 2001; Dembczyński et al., 2010). Given a training set of size n, $\{(\boldsymbol{x}_1, y_1), \ldots, (\boldsymbol{x}_n, y_n)\}$, where $\boldsymbol{x}_i$ is the input and y_i is the corresponding target, through approximately minimizing the *empirical risk*

$$\hat{L}_\lambda(f) = \frac{1}{n}\sum_{i=1}^{n} l(f(\boldsymbol{x}_i), y_i) + \frac{\lambda\|\mathbf{w}\|^2}{n}, \tag{2}$$

boosting iteratively adds terms into the model and yields a sequence of models $f^{(1)}, \ldots, f^{(k)}$. The last term of equation 2 is the regularization term, $\mathbf{w} = (w_1, \ldots, w_k)^T \in \mathbb{R}^k$ is the weight vector, and $\lambda \geq 0$ is the regularization parameter. Note that l is a loss function derived as shifted negative log likelihood, measuring the cost of outputting $f(\boldsymbol{x}_i)$ while the true value is y_i.

4 METHODOLOGY

4.1 FRAMEWORK DESIGN

Actor implemented with Rule-Based Ensembles: We replace the neural network-based action function approximation with an actor composed of additive rule ensembles. Let $\mathcal{F}(s) = \{f_a(s) : \forall a \in A\}$ represent the collection of ensemble models for action a in the action space A at state $s \in S$. The size for A is m. The ensemble $f_a(s)$ for an action a predicts the expected advantages directly, simplifying its expression as $\mathcal{A}(s, a) = f_a(s)$. This prediction is based on a linear combination of Boolean query functions, weighted by coefficients specific to each action $a \in A$: $f_a(s) = \sum_{j=1}^{k} w_{a,j} q_{a,j}(s)$, where $w_{a,j}$ are the coefficients for $q_{a,j}$. For each action a, there are k Boolean query functions $q_{a,j}, \ \ (j = 1 \ldots, k)$ specific to the action a. The actor's policy, represented as π, is defined by the probability distribution over action values for a given state, which is derived from $\mathcal{F}$ using the softmax function: $\pi(a|s) = \frac{\exp(f_a(s))}{\sum_{f_a \in \mathcal{F}} \exp(f_a(s))}$. The softmax function ensures that $\pi(a|s)$ is a proper probability distribution over the action space.

Critic implemented with Neural Network: In our framework, the critic functions similarly to traditional actor-critic systems, leveraging the computational capabilities of neural networks. It serves as a function approximator, implemented using a neural network that estimates the value of being in a specific state s. This neural network, paramount in computing state-value functions, is parameterized by weights ϕ, and the value function it approximates is denoted by $V_\phi(s)$. This design choice ensures that our critic effectively harnesses the processing power of neural networks to deliver precise value estimations for each state. The pseudocode for the algorithm is shown in Appendix B.

4.2 POLICY UPDATE

Critic Policy Update: The critic in our framework estimates the value function $V(s)$ using a neural network, representing the expected return from a state s. The critic is updated by minimizing the loss function, typically the mean squared error between the estimated value and the target value. The target value is derived from the rewards obtained and the discounted values of subsequent states: $L_V(\phi) = \mathbb{E}\left[\left(R_t + \gamma V(s_{t+1}) - V_\phi(s_t)\right)^2\right]$, where R_t is the reward received after taking action a_t in state s_t, γ is the discount factor, $V_\phi(s_{t+1})$ is the value estimate for the next state, and ϕ are the parameters of the critic network.

Actor Update: The learning process involves iterative updates to the coefficient vector $\mathbf{w}_a$ and the query functions q_a based on observed rewards and state transitions, aiming to refine the ensembles for optimal decision-making. This approach leverages the interpretability of rule-based systems in the actor's policy formulation, enhancing transparency in complex or high-dimensional state spaces. The advantage function, used by the actor for updates, is computed using the critic's value function and the immediate reward: $\mathcal{A}_t(s_t, a_t) = R_t + \gamma V(s_{t+1}) - V(s_t)$. This expression calculates how much better the current action a_t is compared to the average action at state s_t at time t, considering the immediate reward and discounted future values. The actor updates the policy by adjusting the parameters $(\mathbf{w}, \mathbf{q})$ in the direction suggested by the critic's evaluations. The update is guided by the gradient of the policy's performance, which is estimated using the advantage function. The loss function derived from the policy gradient is

$$\nabla L_\lambda(\mathbf{w}, \mathbf{q}) = -\mathbb{E}\left[\nabla_{\mathbf{w},\mathbf{q}} \log \pi(a_t|s_t, \mathbf{w}, \mathbf{q}) \mathcal{A}_t\right] + \lambda \nabla_{\mathbf{w},\mathbf{q}} \|\mathbf{w}\|_2^2. \tag{3}$$

To make the loss function locally convex, we add a regularization term $\lambda\|\mathbf{w}\|_2^2$ to the original loss, where λ is the regularization parameter (see Appendix C). The actor is updated by modifying each rule ensemble model f_a in accordance with the calculated policy gradient objective for each action. To obtain the gradient for each action, we use softmax for action selection, taking the natural logarithm of the policy yields:

$$\forall a \quad \log \pi(a \mid s_t; \mathbf{w}, \mathbf{q}) = \mathbf{w}_a \mathbf{q}_a - \log \sum_{j=1}^{m} \exp(\mathbf{w}_{a_j} \mathbf{q}_{a_j}). \tag{4}$$

Substituting equation 4 into equation 3, we have:

$$\nabla L_\lambda(\mathbf{w}, \mathbf{q}) = -\mathbb{E}\left[\nabla_{\mathbf{w},\mathbf{q}} \mathcal{A}_t \left(\mathbf{w}_{a_t} \mathbf{q}_{a_t} - \log \sum_{j=1}^{m} \exp(\mathbf{w}_{a_j} \mathbf{q}_{a_j})\right)\right] + \lambda \nabla_{\mathbf{w},\mathbf{q}} \|\mathbf{w}\|_2^2. \tag{5}$$

Treating $\mathbf{w}$ and $\mathbf{q}$ as a combined vector $\boldsymbol{\theta} = (\mathbf{w}; \mathbf{q})$, the gradient of $\nabla_{\boldsymbol{\theta}} L(\mathbf{w}, \mathbf{q})$, i.e., $\nabla^2_{\boldsymbol{\theta}} L(\mathbf{w}, \mathbf{q})$ can be derived as

$$\nabla^2_{\boldsymbol{\theta}} L_\lambda(\mathbf{w}, \mathbf{q}) = \frac{\partial \nabla l}{\partial \mathbf{w}_a \mathbf{q}_a} = -\mathbb{E}\left[\nabla_{w_a, q_a} \frac{\mathcal{A}_t \partial}{\partial \mathbf{w}_a \mathbf{q}_a} \left(\mathbf{w}_{a_t} \mathbf{q}_{a_t} - \log \sum_{j=1}^{m} \exp(\mathbf{w}_{a_j} \mathbf{q}_{a_j})\right)\right] =$$

$$-\mathbb{E}\left[\nabla_{w_a, q_a} \mathcal{A}_t \left(\mathbb{I}_{a=a_t} - \frac{\exp(\mathbf{w}_a \mathbf{q}_a)}{\sum_{j=1}^{m} \exp(\mathbf{w}_{a_j} \mathbf{q}_{a_j})}\right)\right] = -\mathbb{E}\left[\nabla_{w_a, q_a} \mathcal{A}_t \left(\mathbb{I}_{a=a_t} - \pi(a \mid s_t; \mathbf{w}, \mathbf{q})\right)\right].$$

Taking into account the two distinct situations $a = a_t$ and $a \neq a_t$, the policy gradient for each rule ensemble is as follows:

1. When the ensemble model f_a corresponds to the action executed in the current step, i.e., $a = a_t$,
$$\nabla^2_{w_a, q_a} L_\lambda(w_a, q_a) = \mathbb{E}\left[-\nabla_{w_a, q_a} \mathcal{A}(s_t, a_t)(1 - \pi(a_t|s))\right]; \tag{6}$$
2. When the ensemble model f_{a_i} does not correspond to the action selected by the actor at that time step, i.e., $a \neq a_t$,
$$\nabla^2_{w_a, q_a} L_\lambda(w_a, q_a) = \mathbb{E}\left[\nabla_{w_a, q_a} \mathcal{A}(s_t, a_t)\pi(a_t|s))\right]. \tag{7}$$

This distinction ensures ensemble updates properly align with the actions taken, enabling targeted adjustments that enhance the actor's policy based on observed outcomes and predicted advantages.

Detailed Rule Update:

Step 1: In time-step t, for f_a, we first **select a new query** q_t from a candidate set $\mathcal{Q}$ by solving

$$q_t = \arg\max_{q \in \mathcal{Q}} \text{obj}\big(q; f_a^{(t-1)}\big), \tag{8}$$

where we adopt OGB (Yang et al., 2024) for the objective function. Let $\boldsymbol{q} = (q(\boldsymbol{x_1}), \ldots, q(\boldsymbol{x_n}))^T \in \{0,1\}^n$ is the query vector of the query q, and $\boldsymbol{g}^{(t-1)} = (\partial L_\lambda(f_a^{(t-1)})/\partial f_a^{(t-1)}(\boldsymbol{x}_1), \ldots, \partial L_\lambda(f_a^{(t-1)})/\partial f_a^{(t-1)}(\boldsymbol{x}_n))^T$ is the gradient vector of the empirical risk with respect to the predicted values of $f_a^{(t-1)}$. $\boldsymbol{g}_\perp^{(t-1)}$ and $\boldsymbol{q}_\perp$ are the projection of $\boldsymbol{g}$ and $\boldsymbol{q}$ onto the orthogonal complement of the range of $\boldsymbol{Q}_{t-1} = (\boldsymbol{q}_1, \ldots, \boldsymbol{q}_{t-1})^T$, where $\boldsymbol{q}_i = (q_i(\boldsymbol{x_1}), \ldots, q_i(\boldsymbol{x_n}))^T \in \{0,1\}^n$ is the query vector of the query q_i for $i = 1, \ldots, t-1$. We express the objective function as follows: $\text{obj}(q; f_a^{(t-1)}) = \text{obj}_{\text{ogb}}(q) = |\boldsymbol{q}_\perp^T \boldsymbol{g}_\perp^{(t-1)}|/\|\boldsymbol{q}_\perp\|$. The candidate query set $\mathcal{Q}$ comprises all possible conjunctions of propositions, where each proposition corresponds to a condition that splits the attribute space based on attribute values of given data points (e.g., threshold-based splits). The objective function is maximized using greedy or beam search.

Step 2: After adding the updated new query, we re-calculate the optimal weight vector by solving

$$\mathbf{w}_t = \arg\min_{\mathbf{w} \in \mathbb{R}^t} \hat{L}_\lambda\Big(\boldsymbol{Q}_t, \mathbf{w}\Big), \tag{9}$$

where $\mathbf{Q}_t = \mathbf{Q}_{t-1} \cup \boldsymbol{q}_t$ is the $n \times t$ matrix with the outputs of the selected queries.

Step 3: After there are k rules in the system, instead of continuing to add a new rule for each time, we adopt the **post-processing replacement** step of boosting algorithm (Shalev-Shwartz et al., 2010). In each iteration, we remove one rule with minimal absolute weight, leaving $k-1$ rules in the model: $k^\star = \arg\min_{1\le r\le k}|w_r|$, and remove the query function $q_{k^\star}$ together with its coefficient $w_{k^\star}$, thereby reducing the ensemble to $f^{(k^-)}$ with $k-1$ terms. Then, we need to recompute the weight vector $\mathbf{w}_{k^-} = (w_r)^T_{r\in[k],r\neq k^\star}$ ([k]={1,...,k}) of $f^{(k^-)}$ along with the updated query functions $\{q_r\}_{r\in[k],r\neq k^\star}$: $\mathbf{w}_{k^-} = \arg\min_{\mathbf{w}\in\mathbb{R}^{k-1}} \hat{L}_\lambda\Big(\mathbf{Q}_{k^-}, \mathbf{w}\Big)$, where $\mathbf{Q}_{k^-} = \{q_r\}_{r\in[k],r\neq k^\star}$ is the $n \times (k-1)$ matrix with the outputs of the selected queries.

Step 4: After this, repeat *Step 1* to add a new rule to the system. In the end, the weights of all the k rules are recalculated (same as 8 and 9) in *Step 2*. If the expected loss does not decrease after the post-processing procedure, the model before post-processing is restored. The performance of the post-processing with fully-corrective boosting is guaranteed by the following theorem.

4.3 Theoretical Analysis

We present a comprehensive theoretical convergence analysis of our NSAC algorithm. Under standard assumptions, our algorithm converges to a local optimum. We assume the following conditions:

Assumption 4.1 (Step Sizes)**.** Assume $\alpha_{(\mathbf{w},\mathbf{q})}$ be the learning rate for actor and let α_ϕ be the learning rate for the critic. The sequences $\{\alpha_\phi(t)\}$ and $\{\alpha_{(\mathbf{w},\mathbf{q})}(t)\}$ are positive and satisfy

$$\sum_{t=0}^{\infty}\alpha_\phi(t)=\infty,\quad \sum_{t=0}^{\infty}\alpha_{(\mathbf{w},\mathbf{q})}(t)=\infty, \sum_{t=0}^{\infty}\big(\alpha_\phi(t)^2+\alpha_{(\mathbf{w},\mathbf{q})}(t)^2\big)<\infty,\quad \lim_{t\to\infty}\frac{\alpha_{(\mathbf{w},\mathbf{q})}(t)}{\alpha_\phi(t)} = 0,$$

so that the critic update occurs on a faster timescale.

Assumption 4.2 (Markovian Sampling & Ergodicity)**.** We assume mild mixing or ergodicity conditions ensuring that each state-action pair is visited infinitely often in the limit, and that standard stochastic approximation methods apply.

Assumption 4.3. We assume a Lipschitz-smooth approximator for $V_\phi(s)$. We assume the "compatibility" holds or that any residual bias in the critic's estimate does not prevent recovering the true gradient direction in expectation.

Theorem 4.4. *(Theorem 2.9 in (Shalev-Shwartz et al., 2010)) Let $L(f)$ be the risk function defined by a β-smooth loss function, where the expectation is with respect to an arbitrary distribution over $X\times Y$. Let $\lambda>0$ be a scalar, f is an additive rule ensemble with k rules, $\bar{f}$ is a reference rule ensemble with k_0 rules, if $k+1\ge k_0(1+16/\lambda^2)$, and assume that L is $(k+1+k_0,\lambda)$-sparsely-strongly convex. Additionally, let τ be an integer such that*

$$\tau \ge \frac{\lambda(k+1-k_0)}{2\beta}\log\left(\frac{L(0)-L(\bar{f})}{\epsilon}\right). \tag{10}$$

Then if the fully corrective boosting is run for k iterations and its last predictor is provided as input for the post-processing replacement procedure, which is then run for τ iterations, then when the procedure terminates at time t, we have $L(f^{(t)})-L(\bar{f})\le\epsilon$.

Theorem 4.5. *Let ϕ be the fixed parameters of a critic, inducing a fixed value function $V_\phi(s)$ for each state $s\in\mathcal{S}$. Let f be a parameterized function (e.g., the actor's approximation to the advantage) that is updated iteratively according to the update rule, the sequence $\{f_k\}$ converges to $\bar{f}$.*

Proof. We first calculate the risk for rule ensembles for $\bar{f}$ and f_k based on the loss functions: $L(\bar{f}) = -\log\pi_{\bar{f}}(a_t|s_t)\bar{f}$ and $L(f_k) = -\log\pi_{f_k}(a_t|s_t)f_k$, respectively. When $R(\cdot)$ is error bounded, there exists a lower bound with a constant $\gamma>0$ satisfying $\big|L(f_1)-L(f_2)\big| \ge \gamma\|f_1-f_2\|$, for any f_1 and f_2 in the parameter space. Based on Theorem 4.4, when equation 10 is satisfied, we have $\|f_k-\bar{f}\| \le \frac{1}{\gamma}\big|L(f_k)-L(\bar{f})\big| \le \frac{\varepsilon}{\gamma}$. Hence, bounding the difference in risk $|L(f_k)-L(\bar{f})|$ by ε forces the parameter distance $\|f_k-\bar{f}\|$ to lie within $\frac{\varepsilon}{\gamma}$. □

Theorem 4.6 (Convergence of NSAC). *Let $\{(w_t, q_t), \phi_t\}$ be the sequence of actor and critic parameters updated via Eqs. equation 6–equation 7 under the Assumptions 4.1–4.3. Then $\{(w_t, q_t), \phi_t\}$ converges* almost surely *to a set of stationary points of the associated ordinary differential equation (ODE) system: $\dot{\phi} = F(\phi; (\mathbf{w}, \mathbf{q})), (\dot{w}, \dot{q}) = G((\mathbf{w}, \mathbf{q}); \phi)$ where F represents the temporal-difference (critic) dynamics, and G represents the policy-gradient (actor) dynamics. In particular, (w, q) converges to a* local optimum *of $J(w, q)$, where J is the expected cumulative reward.*

Proof. We employ the concepts of *Two-timescale* theorems (Borkar & Meyn, 2000; Wu et al., 2020) and Theorem 4.5 for the proof. Please refer to Appendix D for the detailed proof of convergence. □

Computational Complexity: This algorithm has a time complexity of $O(d^2nk)$ per rule, where d is the number of attributes. It performs at most d iterations to construct a single rule (adding one attribute per iteration), and in each iteration, it evaluates all d attributes as candidates. The bottleneck lies in computing the orthogonal gradient boosting objective $\text{obj}_{\text{ogb}}(q) = |g^T q|/(||q_\perp|| + \epsilon)$ for each candidate, which requires $O(nk)$ operations due to the orthogonal projection computation: $g_\perp = g - BB^T g$. This represents a k-fold increase in computational cost over standard gradient boosting (which has complexity $O(d^2n)$). The orthogonalization overhead is essential for the algorithm's ability to select more general rules and achieve better risk-complexity trade-offs in practice. Fully-corrective weight calculation has a complexity of $O(k^2n)$ from solving a convex optimization problem that re-optimizes all rule weights after adding each new rule. The k^2 scaling comes from computing the Hessian on the $k \times k$ Gram matrix Q^TQ. While more expensive than stage-wise approaches, this cost is manageable for small ensemble sizes typically in interpretable rule learning.

5 Experiments and Results

We evaluated the performance of NSAC in five diverse RL environments: MountainCar-v0, Acrobot-v1, CartPole-v1, Blackjack-v1, and Postman (Sutton, 2018; Dietterich, 2000). We also evaluated our NSAC algorithm on a challenging, real-world HVAC control benchmark using Sinergym. This environment models a multi-zone office building with coupled thermal dynamics, where each zone's temperature, humidity, and carbon dioxide concentration evolve according to nonlinear heat-transfer and air-exchange equations. Control actions, such as heating and cooling set points, must be chosen every 15 minutes to balance energy consumption against comfort constraints under stochastic disturbances (varying weather, occupancy schedules) and long planning horizons. Our reward function balances occupant comfort against energy use, encouraging high comfort with minimal energy consumption. The high dimensionality of the state–action space, the strong inter-zone couplings, and the requirement to satisfy strict comfort bands make this task a great testbed for our algorithm. We conducted a comprehensive performance comparison against established benchmark algorithms, including Q-Tabular (Sutton, 2018), DQN (Mnih, 2013), PPO (Schulman et al., 2017), and A2C (Mnih et al., 2016), all implemented using Stable-Baselines3 (Raffin et al., 2021). We additionally included Rainbow (Hessel et al., 2018), SDSAC (Kong et al., 2021), and SACBBF (Zhang et al., 2024) as deep RL baselines. To cover symbolic approaches, we also evaluated three interpretable methods: SYMPOL (Marton et al., 2024), $\pi_{\textit{affine}}$-D (Qiu & Zhu, 2022), and D-SDT (Silva et al., 2020). For a fair comparison, we use the Gym environments in their original form without any modifications. For each algorithm, we apply the recommended optimal parameters provided by the RLzoo (Raffin & contributors, 2020) with Stable Baselines 3.

Performance Evaluation: As shown in Table 1, NSAC demonstrates strong and reliable performance across a wide spectrum of tasks, outperforming or matching both classic deep RL methods and symbolic approaches. Compared with classical methods such as Q-learning, DQN, A2C, PPO, SAC variants, and Rainbow, NSAC achieves consistently higher returns with lower variance, particularly in settings that demand stability and scalability. Unlike value-based methods that can be brittle in continuous or high-dimensional domains, NSAC maintains robustness while still being competitive in simpler benchmarks. Against symbolic methods such as SYMPOL, $\pi_{\textit{affine}}$-D, and D-SDT, NSAC shows even clearer advantages: while symbolic policies can excel on select tasks due to strong inductive biases, they often suffer from collapse or sharp degradation when scaled, whereas NSAC delivers stable performance across all environments. These results highlight NSAC's ability to combine the adaptability and generalization strength of neural methods with symbolic reliability.

Table 1: Comparison of Various Methods with Our Approach Across RL Environments.

Environment	Q-table	DQN	A2C	PPO	SDSAC	SACBBF	Rainbow	SYMPOL	π_{affine}-D	D-SDT	NSAC
MCar-v0	-147.68 ± 9.52	*-135.07* ± 16.42	-157.51 ± 37.12	-150.40 ± 4.05	-141.76 ± 13.91	-139.23 ± 17.62	-137.76 ± 39.47	-200 ± 0	-200 ± 0	-200 ± 0	**-132.25** ± 16.08
Acrobot-v1	-201.01 ± 13.32	-112.68 ± 8.93	-98.931 ± 29.52	*-82.629* ± 2.79	-85.124 ± 7.82	-88.708 ± 7.12	-89.753 ± 8.98	**-80.02** ± 4.28	-425.47 ± 56.81	-212.31 ± 4.19	-87.714 ± 6.95
CartPole-v1	219.51 ± 69.2	161.00 ± 55.2	453.51 ± 92.5	498.73 ± 2.4	487.61 ± 2.71	481.07 ± 10.76	498.53 ± 2.12	**500** ± 0	109 ± 76.82	498.53 ± 2.12	*499.14* ± 1.91
Blackjack-v1	**-0.06** ± 0.02	**-0.06** ± 0.02	-0.07 ± 0.01	**-0.06** ± 0.01	-0.07 ± 0.02	**-0.06** ± 0.01	**-0.06** ± 0.02	**-0.06** ± 0.01	-0.08 ± 0.01	-0.08 ± 0.02	**-0.06** ± 0.01
Postman	**35.24** ± 2.06	31.91 ± 5.71	24.23 ± 3.09	34.35 ± 3.82	*34.91* ± 2.86	31.12 ± 3.77	34.67 ± 4.68	25.34 ± 3.42	15.23 ± 4.91	18.91 ± 6.28	27.14 ± 3.38
HVAC-1Zone	NA	-1445367 ± 20183	*-1334562* ± 148658	-1865276 ± 135683	-1387692 ± 145619	-1423573 ± 34825	-1465732 ± 785732	-1478783 ± 65293	-1895286 ± 42873	-1862537 ± 29763	**-1251321** ± 85241
HVAC-5Zone	NA	-1876253 ± 198263	-1984843 ± 287237	-1676288 ± 462837	-1582742 ± 227221	*-1547279* ± 241625	-1602142 ± 342612	-1586352 ± 65792	-1969635 ± 45241	-1876374 ± 33468	**-1463601** ± 121678

Note. ***Bold*** *indicates the best performance across all benchmarks.* *Underscore* *denotes the second-best performance.* *Red* *highlights the best-performing method among symbolic-based approaches.*

This makes it a practical and effective alternative that closes the gap between the strengths of classic RL and symbolic reasoning while avoiding their respective weaknesses.

Interpretability Evaluation: We also evaluate the interpretability of our method. Common evaluation metrics for interpretable models include fidelity, comprehensibility, and cognitive load. In our approach, measuring fidelity is unnecessary because it is primarily relevant in post-hoc explanation settings—where one model attempts to approximate and explain the behavior of another. In contrast, our model is inherently self-explainable, meaning it achieves 100% fidelity by design, as the decisions made by the model directly reflect its underlying logic. For comprehensibility and cognitive load, our rule-based system offers a structured and measurable format. The additive rule ensembles consist only of boolean propositions formed through simple comparisons (e.g., feature $>$ threshold) and logical conjunctions. In general, comprehensibility is negatively correlated with model complexity, while cognitive load increases with complexity. We define model complexity in terms of the total number of rules, conditions, and logical operations. Models with more parameters and operations tend to be harder to understand and place a greater cognitive burden. Since the performance of π_{affine}-D, and D-SDT is not directly comparable, we instead evaluate them in terms of interpretability. Using model size as a proxy for complexity, we observe that across all environments our models require, on average, 61.23 parameters to achieve the reported performance. In contrast, SYMPOL uses 95.6 parameters (approximately one per node).

Human Interpretability Analysis - MountainCar: In this section, we use the MountainCar-v0 environments from OpenAI Gym as examples to illustrate the interpretability of our proposed reinforcement learning algorithm. The Mountain Car environment involves a car situated between two hills, tasked with reaching the flag at the top of the right hill. Due to insufficient engine power, the car must build momentum by oscillating back and forth. The system state is characterized by two continuous variables: the car's position (p) and its velocity (v). The agent performs one of three discrete actions: push left, do nothing, or push right. For each action, a set of rules evaluate the current state by applying specific conditions based on p and v, assigning corresponding scores that influence the decision-making process. Consider a typical state where $p = -0.5$ (slightly to the left of the center) and $v = 0.02$ (moving rightward). For the action *Do Nothing*, one rule imposes a penalty of -13.4848 since the velocity v exceeds a small positive threshold, discouraging inaction that could result in insufficient momentum to overcome the hill. For the action *Push Left*, only one rule applies, which assigns a posi-

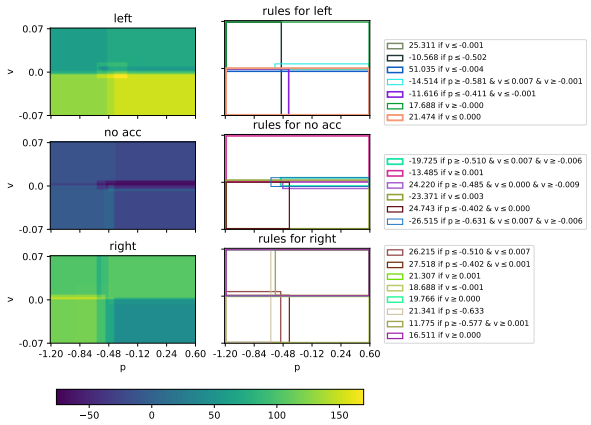

Figure 2: Visual representation of the rules for MountainCar.

tive score as the velocity v is above a minimal threshold, encouraging a slight push left to maintain momentum without overcompensating. Conversely, the action *Push Right* activates multiple rules: three contribute $+57.59$ because the velocity v surpasses different threshold values for the corresponding rules, strongly encouraging a push right to build momentum; another rule provides $+11.7750$ since both the position $p \geq -0.5768$ and velocity is positive are satisfied, indicating that a rightward push is beneficial without risking overshooting the valley; There is also one rule contributing an additional $+1.3610$ because the position $p \leq -0.4494$, $p \geq -0.8744$, and $v \leq 0.0234$ hold true, subtly encouraging a push right to maintain the car within a stable range. The cumulative score for *Push Right* thus amounts to $+70.7247$, clearly favoring this action. This comprehensive rule-based scoring system demonstrates that, for the given state ($p = -0.5$, $v = 0.02$), pushing right is the optimal choice as it significantly builds the necessary momentum to ascend the hill, outweighing the moderate incentives to push left and the discouragement from doing nothing. We have also visualized the rules of MountainCar in Figure 2 with all rules presented in Appendix L. One can easily identify the corresponding areas associated with a state and locate the applicable rules.

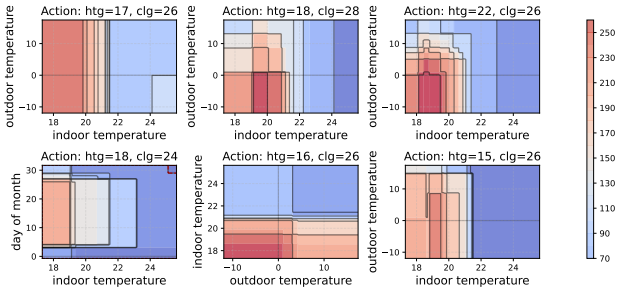

Figure 3: Visualization of the HVAC Rules

Human Interpretability Analysis - Real Time HVAC control: Alongside standard Gym benchmarks, we evaluated our algorithm on a challenging, real-world HVAC control problem in a biological laboratory, where maintaining temperature within a narrow band is vital to preserving the viability of cultured viruses.In such safety-critical settings, interpretability is crucial: when RL governs biocontainment HVAC systems, even minor errors can destroy cultures or compromise containment. As shown in Table 1, our rule-based actor approach delivers performance nearly equal to—or even surpassing—that of traditional baseline methods. More than this, our proposed algorithm also delivers interpretability by explaining why and how each decision is made in human-understandable language, enabling users to assess the correctness of its rules. Consider the very first rule as an example: *if outdoor temperature* ≤ -4.5*; htg setpoint* ≤ 20.0*; air temperature* ≤ 21.1503*, and HVAC electricity demand rate* $\geq 1452.0250(kW)$*, +37.6076* What it means, in plain English: When all four of these conditions hold: 1. Outdoor temperature is extremely low; 2. The heating setpoint remains at a moderate level; 3. The indoor air temperature is still below the desired comfort threshold; 4. The HVAC system is already drawing high power, then this rule "fires," adding +37.6 to the score for choosing (htg = 15 degree, clg = 26 degree)—i.e., heat turns on below 15 °C and cooling above 26 °C. A large positive weight like +37.6 signifies that, in this scenario, raising the heating setpoint to 15 °C is especially beneficial. Based on visualized the rules of HVAC control in Figure 3, when it's freezing outside, your target heating level is still under typical comfort, the room hasn't yet warmed up, and the system is working hard—so raising the heat setpoint to 15 degree markedly improves comfort, which this rule captures (see details in Appendix J).

6 Discussion and Conclusion

Like all other self-interpretable methods, there is an inherent trade-off between interpretability and performance. A more complex state space may require a greater number of rules to describe it, and while an increased rule count can potentially enhance performance, it may significantly reduce interpretability. The optimal number of rules varies, depending on specific environments and applications. We may need to carefully select the right number of rules for each task, just like fine-tuning a neural network's hyperparameters. However, based on our experimental results, 10-15 rules are sufficient to address most scenarios. In conclusion, this paper introduces a neural+symbolic approach within the actor-critic framework. This method leverages both the robust function approximation capabilities of neural networks critic and the interpretability provided by rule-based actor models. Users can trace how and why the model makes each decision and evaluate its reasoning. In the future, we plan to assess the scalability of our method in more complex environments across different domains, such as robotics, finance, healthcare, or autonomous driving, and adapt with other actor-critic frameworks, such as Soft Actor-Critic.

Ethical Statement

This work does not involve human subjects, personal data, or identifiable information. All experiments are conducted entirely in simulated environments, including stylized energy-system tasks designed to probe safety and performance trade-offs. These simulations do not interface with or control any real-world infrastructure. Our proposed NSAC framework aims to improve the interpretability and trustworthiness of reinforcement learning systems by combining symbolic rules with statistical learning. This direction supports the broader goal of promoting transparency in AI decision-making. While the symbolic actor promotes explainability, we acknowledge the importance of careful rule design to avoid unintended consequences in safety-critical domains. However, our current implementation is strictly research-oriented and intended for controlled, offline evaluation.

Reproducibility Statement

To support reproducibility, we include comprehensive details of our training procedures, hyperparameter settings, and evaluation metrics within the main text and appendix. Upon publication, we will release the full codebase, including: Random seeds and environment specifications, Training scripts to replicate all experiments, Plotting utilities to reproduce all figures. All results can be reproduced using a single command-line interface without manual intervention. Pretrained models and logs will also be provided to facilitate benchmarking and verification.

References

Osbert Bastani, Yewen Pu, and Armando Solar-Lezama. Verifiable reinforcement learning via policy extraction. In *NeurIPS*, 2018.

José Manuel Benítez, Juan Luis Castro, and Ignacio Requena. Are artificial neural networks black boxes? *IEEE Transactions on neural networks*, 8(5):1156–1164, 1997.

Vivek S Borkar and Sean P Meyn. The ode method for convergence of stochastic approximation and reinforcement learning. *SIAM Journal on Control and Optimization*, 38(2):447–469, 2000.

Davide Castelvecchi. Can we open the black box of ai? *Nature News*, 538(7623):20, 2016.

Yannick Coppens, Konstantinos Efthymiadis, Tom Lenaerts, and Ann Nowé. Distilling deep reinforcement learning policies in soft decision trees. In *IJCAI Workshop on Explainable Artificial Intelligence (XAI)*, 2019.

Krzysztof Dembczyński, Wojciech Kotłowski, and Roman Słowiński. Ender: a statistical framework for boosting decision rules. *Data Mining and Knowledge Discovery*, 21(1):52–90, 2010.

Thomas G Dietterich. Hierarchical reinforcement learning with the maxq value function decomposition. *Journal of artificial intelligence research*, 13:227–303, 2000.

Zihan Ding, Pablo Hernandez-Leal, Gavin Weiguang Ding, Changjian Li, and Ruitong Huang. Cdt: Cascading decision trees for explainable reinforcement learning. *arXiv preprint arXiv:2011.07553*, 2020.

Damien Ernst, Pierre Geurts, and Louis Wehenkel. Tree-based batch mode reinforcement learning. *Journal of Machine Learning Research*, 6(Apr):503–556, 2005.

Jerome H Friedman. Greedy function approximation: a gradient boosting machine. *Annals of statistics*, pp. 1189–1232, 2001.

Jerome H Friedman and Bogdan E Popescu. Predictive learning via rule ensembles. *The annals of applied statistics*, 2(3):916–954, 2008.

Artur d'Avila Garcez, Aimore Resende Riquetti Dutra, and Eduardo Alonso. Towards symbolic reinforcement learning with common sense. *arXiv preprint arXiv:1804.08597*, 2018.

Jayesh K Gupta, Maxim Egorov, and Mykel Kochenderfer. Cooperative multi-agent control using deep reinforcement learning. In *Proceedings of the International Conference on Autonomous Agents and Multiagent Systems (AAMAS)*, 2015a.

Ujjwal Das Gupta, Erik Talvitie, and Michael Bowling. Policy tree: Adaptive representation for policy gradient. In *Proceedings of the AAAI Conference on Artificial Intelligence*, volume 29, 2015b.

Daniel Hein, Steffen Udluft, and Thomas A Runkler. Interpretable policies for reinforcement learning by genetic programming. *Engineering Applications of Artificial Intelligence*, 76:158–169, 2018.

Matteo Hessel, Joseph Modayil, Hado Van Hasselt, Tom Schaul, Georg Ostrovski, Will Dabney, Dan Horgan, Bilal Piot, Mohammad Azar, and David Silver. Rainbow: Combining improvements in deep reinforcement learning. In *Proceedings of the AAAI conference on artificial intelligence*, volume 32, 2018.

León Illanes, Xi Yan, Rodrigo Toro Icarte, and Sheila A McIlraith. Symbolic plans as high-level instructions for reinforcement learning. In *Proceedings of the international conference on automated planning and scheduling*, volume 30, pp. 540–550, 2020.

Yiting Kong, Yang Guan, Jingliang Duan, Shengbo Eben Li, Qi Sun, and Bingbing Nie. Decision-making under on-ramp merge scenarios by distributional soft actor-critic algorithm. *arXiv preprint arXiv:2103.04535*, 2021.

Mikel Landajuela, Brenden K Petersen, Sookyung Kim, Claudio P Santiago, Ruben Glatt, Nathan Mundhenk, Jacob F Pettit, and Daniel Faissol. Discovering symbolic policies with deep reinforcement learning. In *International Conference on Machine Learning*, pp. 5979–5989. PMLR, 2021.

Guiliang Liu, Oliver Schulte, Wang Zhu, and Qingcan Li. Toward interpretable deep reinforcement learning with linear model u-trees. In *Machine Learning and Knowledge Discovery in Databases: European Conference, ECML PKDD 2018, Dublin, Ireland, September 10–14, 2018, Proceedings, Part II 18*, pp. 414–429. Springer, 2019.

Scott M Lundberg and Su-In Lee. A unified approach to interpreting model predictions. *Advances in neural information processing systems*, 30, 2017.

Daoming Lyu, Fangkai Yang, Bo Liu, and Steven Gustafson. Sdrl: interpretable and data-efficient deep reinforcement learning leveraging symbolic planning. In *Proceedings of the AAAI Conference on Artificial Intelligence*, volume 33, pp. 2970–2977, 2019.

Sascha Marton, Tim Grams, Florian Vogt, Stefan Lüdtke, Christian Bartelt, and Heiner Stuckenschmidt. Mitigating information loss in tree-based reinforcement learning via direct optimization. *arXiv preprint arXiv:2408.08761*, 2024.

Volodymyr Mnih. Playing atari with deep reinforcement learning. *arXiv preprint arXiv:1312.5602*, 2013.

Volodymyr Mnih, Adria Puigdomenech Badia, Mehdi Mirza, Alex Graves, Timothy Lillicrap, Tim Harley, David Silver, and Koray Kavukcuoglu. Asynchronous methods for deep reinforcement learning. In *International conference on machine learning*, pp. 1928–1937. PmLR, 2016.

W James Murdoch, Chandan Singh, Karl Kumbier, Reza Abbasi-Asl, and Bin Yu. Definitions, methods, and applications in interpretable machine learning. *Proceedings of the National Academy of Sciences*, 116(44):22071–22080, 2019.

Wenjie Qiu and He Zhu. Programmatic reinforcement learning without oracles. In *The Tenth International Conference on Learning Representations*, 2022.

Antonin Raffin and contributors. RL Baselines3 Zoo. `https://github.com/DLR-RM/rl-baselines3-zoo`, 2020. Accessed: YYYY-MM-DD.

Antonin Raffin, Ashley Hill, Adam Gleave, Anssi Kanervisto, Maximilian Ernestus, and Noah Dormann. Stable-baselines3: Reliable reinforcement learning implementations. *Journal of Machine Learning Research*, 22(268):1–8, 2021. URL http://jmlr.org/papers/v22/20-1364.html.

Aaron M Roth, Nicholay Topin, Pooyan Jamshidi, and Manuela Veloso. Conservative q-improvement: Reinforcement learning for an interpretable decision-tree policy. *arXiv preprint arXiv:1907.01180*, 2019.

Cynthia Rudin. Stop explaining black box machine learning models for high stakes decisions and use interpretable models instead. *Nature Machine Intelligence*, 1(5):206–215, 2019.

Robert E Schapire. The strength of weak learnability. *Machine learning*, 5(2):197–227, 1990.

John Schulman, Filip Wolski, Prafulla Dhariwal, Alec Radford, and Oleg Klimov. Proximal policy optimization algorithms. *arXiv preprint arXiv:1707.06347*, 2017.

Shai Shalev-Shwartz, Nathan Srebro, and Tong Zhang. Trading accuracy for sparsity in optimization problems with sparsity constraints. *SIAM Journal on Optimization*, 20(6):2807–2832, 2010.

Andrew Silva, Matthew Gombolay, Taylor Killian, Ivan Jimenez, and Sung-Hyun Son. Optimization methods for interpretable differentiable decision trees applied to reinforcement learning. In *International conference on artificial intelligence and statistics*, pp. 1855–1865. PMLR, 2020.

Richard S Sutton. Reinforcement learning: An introduction. *A Bradford Book*, 2018.

Yebin Tao, Lu Wang, and Daniel Almirall. Tree-based reinforcement learning for estimating optimal dynamic treatment regimes. *The annals of applied statistics*, 12(3):1914, 2018.

Yue Frank Wu, Weitong Zhang, Pan Xu, and Quanquan Gu. A finite-time analysis of two time-scale actor-critic methods. *Advances in Neural Information Processing Systems*, 33:17617–17628, 2020.

Fan Yang, Pierre Le Bodic, Michael Kamp, and Mario Boley. Orthogonal gradient boosting for simpler additive rule ensembles. In *International Conference on Artificial Intelligence and Statistics*, pp. 1117–1125. PMLR, 2024.

Le Zhang, Yong Gu, Xin Zhao, Yanshuo Zhang, Shu Zhao, Yifei Jin, and Xinxin Wu. Generalizing soft actor-critic algorithms to discrete action spaces. In *Chinese Conference on Pattern Recognition and Computer Vision (PRCV)*, pp. 34–49. Springer, 2024.

A LIMITATION AND FUTURE WORK

A fundamental limitation of our approach lies in the natural trade-off between interpretability and performance. While our symbolic, rule-based actor offers clear advantages in terms of transparency and simulatability, this structure inherently constrains policy expressiveness compared to fully neural counterparts—particularly in complex, high-dimensional environments. Although NSAC achieves competitive performance across benchmark tasks, there may be scenarios where its symbolic policy cannot match the nuanced optimisation achievable by deep learning-based policies.

Moreover, interpretability is not a binary property but exists on a spectrum. Different symbolic approaches offer varying degrees of clarity, modularity, and simulatability, often depending on the complexity of the rule structure, the nature of the environment, and the domain-specific knowledge embedded within the rules. As such, the perceived interpretability of a symbolic method may vary across users and use cases. Practitioners must therefore carefully consider the type and level of interpretability required for their application—balancing traceability with scalability—when choosing or designing a symbolic component. Future work may explore adaptive symbolic structures or hybrid neuro-symbolic policy representations to better navigate this trade-off across diverse tasks.

B ALGORITHM

Algorithm 1 Neural+Symbolic Actor-Critic Algorithm

Initialize actor with each action rule ensemble function $f_a^{(0)} = 0$
Initialize critic network $V(s, \phi)$ with parameters ϕ
Initialize environment and observe initial state s
repeat
  for each step of episode **do**
    Choose action $a \sim \pi(a|s, \theta)$
    Execute action a in the environment
    Observe reward r and new state s'
    Calculate $\delta = r + \gamma V(s', \phi) - V(s, \phi)$
    Update critic by minimizing $L(\phi) = \delta^2$
    for all a_i in action space **do**
      if $a_i = a$ **then**
        Calculate policy gradient $\boldsymbol{g}_t$: $-\nabla_{\mathbf{w},\mathbf{q}}(1 - \log \pi(a|s, \mathbf{w}^T\mathbf{q}))\delta$ for f_a
      else
        Calculate policy gradient $\boldsymbol{g}_t$: $\nabla_{\mathbf{w},\mathbf{q}} \log \pi(a|s, \mathbf{w}^T\mathbf{q})\delta$ for f_a
      end if
      use Rule Replacement Steps and policy gradient to find a new query for f_a
      use OGB to update the for f_a
    end for
    $s \leftarrow s'$
  end for
  if end of episode **then**
    Reset environment and observe initial state s
  end if
until convergence or maximum episodes reached.

C ACTOR'S LOSS WITH L2 REGULARIZATION

Theorem C.1 (Local Strong Convexity of Actor's Loss with L2 Regularization)**.** *Consider the actor's loss function in an A2C framework defined as*

$$L(\theta) = -\mathbb{E}_{s\sim\rho^\pi, a\sim\pi_\theta}\left[A^\pi(s,a)\log\pi_\theta(a|s)\right] + \frac{\lambda}{2}\|\theta\|^2,$$

where $\lambda > 0$ is the regularization coefficient for L2 regularization.

We assume:

Algorithm 2 Orthogonal Gradient Boosting (OGB)

Input: data $(\boldsymbol{x}_i, y_i)$, number of rules k and $\boldsymbol{g}_t$
$f^{(0)} = 0$
for $t = 1, \ldots, k$ **do**
  $\boldsymbol{q}_t = \arg\max_q |\boldsymbol{g}_{\perp t}^T \boldsymbol{q}| / \|\boldsymbol{q}_\perp\|$
  $\mathbf{w}^{(t)} = \arg\min_{(w_1,\ldots,w_t)\in\mathbb{R}^t} \hat{L}_\lambda(\sum_{j=1}^t w_j q_j)$
  $f^{(t)}(\cdot) = w_1^{(t)} q_1(\cdot) + \cdots + w_t^{(t)} q_t(\cdot)$
end for
Output: $f^{(k)}$

Algorithm 3 Rule Replacement Steps

Input: data $(\boldsymbol{x}_i, y_i)$, $i = 1, \ldots, n$, original rule ensemble with k rules $f_k^{(0)}$, maximum iteration number T and $\boldsymbol{g}$
for $t = 1, \ldots, T$ **do**
  Find the index of the smallest weight absolute value $r = \arg\min_{j\in 1,\ldots,k} |w_j^{(t-1)}|$
  $\tilde{\mathbf{w}}^{(t-1)} = \arg\min_{\mathbf{w}\in\mathbb{R}^{k-1}} \hat{L}_\lambda(\sum_{i\in[k]-\{r\}} \tilde{w}_i^{(t-1)} q_i)$
  $\tilde{f}_{k-1}^{(t-1)}(\cdot) = \sum_{i\in[k]-\{r\}} w_i^{(t-1)} q_i(\cdot)$
  Find the query $q_k^{(t)} = \arg\max_q \|q^T \boldsymbol{g}_\perp\| / |q_\perp|$
  $\mathbf{w}^{(t)} = \arg\min_{\mathbf{w}\in\mathbb{R}^k} \hat{L}_\lambda(\sum_{i\in[k]-\{r\}} w_i q_i + w_r q_r^{(t)})$
  Let $\delta = \hat{L}_\lambda(f^{(t)}) - \hat{L}_\lambda(\sum_{i\in[k]-\{r\}} w_i^{(t)} q_i + w_r^{(t)} q_r^{(t)})$
  if $\delta > 0$ **then**
    $f_k^{(t)} = \sum_{i\in[k]-\{r\}} w_i^{(t)} q_i + w_r^{(t)} q_r^{(t)}$
  else
    break
  end if
end for
Output: $f_k^{(t)}$

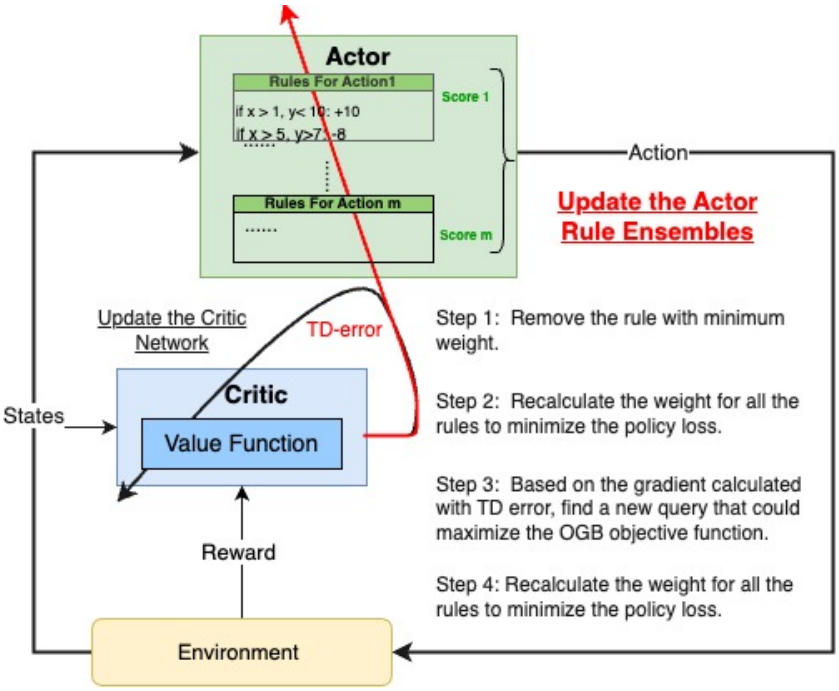

Figure 4: The NSAC Algorithm.

1. *The policy $\pi_\theta(a|s)$ is twice continuously differentiable with respect to θ;*
2. *At a local minimum θ^*, the Hessian of the unregularized loss $L_{unreg}(\theta) = -\mathbb{E}[A^\pi(s,a)\log\pi_\theta(a|s)]$ satisfies $\nabla^2 L_{unreg}(\theta^*) \succeq 0$ (positive semi-definite);*
3. *The regularization coefficient λ is chosen such that $\lambda > 0$.*

Then, there exists a neighborhood $\mathcal{U}$ around θ^* where the regularized loss $L(\theta)$ is strongly convex. Specifically, within $\mathcal{U}$,

$$\nabla^2 L(\theta) \succeq \lambda I,$$

where I is the identity matrix in $\mathbb{R}^{d\times d}$.

Proof. We aim to show that the regularized loss function $L(\theta)$ is strongly convex in a neighborhood around θ^*.

The regularized loss can be expressed as the sum of the unregularized loss and the L2 regularization term:

$$L(\theta) = L_{\text{unreg}}(\theta) + L_{\text{reg}}(\theta),$$

where

$$L_{\text{reg}}(\theta) = \frac{\lambda}{2}\|\theta\|^2.$$

Compute the gradient and Hessian of $L(\theta)$:

$$\nabla L(\theta) = \nabla L_{\text{unreg}}(\theta) + \lambda\theta,$$

$$\nabla^2 L(\theta) = \nabla^2 L_{\text{unreg}}(\theta) + \lambda I.$$

At the local minimum θ^*, by assumption:

$$\nabla^2 L_{\text{unreg}}(\theta^*) \succeq 0.$$

Therefore,

$$\nabla^2 L(\theta^*) = \nabla^2 L_{\text{unreg}}(\theta^*) + \lambda I \succeq \lambda I.$$

This shows that the Hessian of the regularized loss at θ^* is positive definite, as $\lambda > 0$. Since $\pi_\theta(a|s)$ is twice continuously differentiable, $\nabla^2 L_{\text{unreg}}(\theta)$ is continuous in θ. Hence, there exists a neighborhood $\mathcal{U}$ around θ^* where:

$$\nabla^2 L_{\text{unreg}}(\theta) \succeq 0, \quad \forall \theta \in \mathcal{U}.$$

Within $\mathcal{U}$,

$$\nabla^2 L(\theta) = \nabla^2 L_{\text{unreg}}(\theta) + \lambda I \succeq \lambda I.$$

This inequality holds because $\nabla^2 L_{\text{unreg}}(\theta) \succeq 0$ and λI is positive definite. Since $\nabla^2 L(\theta) \succeq \lambda I$ for all $\theta \in \mathcal{U}$, the loss function $L(\theta)$ is **strongly convex** in the neighborhood $\mathcal{U}$ around θ^* with strong convexity parameter λ.

□

Theorem C.2 (Local Error Bound under Local Strong Convexity)**.** *Let $L : \mathbb{R}^d \to \mathbb{R}$ be continuously differentiable and* μ-strongly convex *in a neighborhood $\mathcal{N}$ of some point $\hat{f} \in \mathbb{R}^d$. In other words, there exists $\mu > 0$ such that for all $f \in \mathcal{N}$,*

$$L(f) - L(\hat{f}) \;\geq\; \frac{\mu}{2} \| f - \hat{f} \|^2.$$

Then, for every f in that neighborhood $\mathcal{N}$,

$$\| f - \hat{f} \| \;\leq\; \sqrt{\frac{2}{\mu} \big(L(f) - L(\hat{f}) \big)}.$$

Proof. Since R is μ-strongly convex in the neighborhood $\mathcal{N}$ around $\hat{f}$, we have the inequality

$$L(f) \;-\; L(\hat{f}) \;\geq\; \frac{\mu}{2} \| f - \hat{f} \|^2, \quad \forall f \in \mathcal{N}.$$

Rearrange this to obtain

$$\| f - \hat{f} \|^2 \;\leq\; \frac{2}{\mu} \Big(L(f) - L(\hat{f}) \Big).$$

Taking the square root of both sides yields

$$\| f - \hat{f} \| \;\leq\; \sqrt{\frac{2}{\mu} \Big(L(f) - L(\hat{f}) \Big)}.$$

Thus, in the local region $\mathcal{N}$, a small gap in the objective value $L(f) - L(\hat{f})$ forces f to be close to $\hat{f}$. This is precisely the local *error-bound* property. □

D Proof for Convergence of our Proposed Algorithm

Theorem D.1 (Convergence of our Proposed Algorithm)**.** *Let $\{(w_t, q_t), \phi_t\}$ be the sequence of actor and critic parameters updated via equation 6–equation 7 under the Assumptions 4.1–4.3. Then $\{(w_t, q_t), \phi_t\}$ converges* almost surely *to a set of stationary points of the associated ODE system:*

$$\begin{cases} \dot{\phi} \;=\; F(\phi;\, (\mathbf{w}, \mathbf{q})), \\ (\dot{w}, \dot{q}) \;=\; G((\mathbf{w}, \mathbf{q});\, \phi), \end{cases}$$

where F represents the temporal-difference (critic) dynamics and G represents the policy gradient (actor) dynamics. In particular, (w, q) converges to a local optimum *of $J(w, q)$.*

Proof. By Assumption 4.1, $\alpha_{(\mathbf{w},\mathbf{q})}(t)/\alpha_\phi(t) \to 0$. Hence, on the "fast" timescale, we may treat θ_t as if it were *quasi-static*. Then the critic update is a standard temporal-difference learning procedure (or mean-squared error minimization) *for a fixed policy* $\pi_{(\mathbf{w},\mathbf{q})}$.

From classical TD-learning results (or generalized linear function approximation theory), we know that ϕ_t converges to the set

$$\{\, \phi^*(\mathbf{w}, \mathbf{q}) : F(\phi^*(\mathbf{w}, \mathbf{q})); (\mathbf{w}, \mathbf{q}) = 0 \},$$

provided that $\alpha_\phi(t)$ diminishes appropriately and under the usual conditions.

Formally, one shows that for each fixed $(\mathbf{w}, \mathbf{q})$, the ODE

$$\dot{\phi} = F(\phi;\ (\mathbf{w}, \mathbf{q}))$$

has a globally asymptotically stable equilibrium at $\phi^*(\mathbf{w}, \mathbf{q})$. By the Two-timescale lemma (Borkar & Meyn, 2000; Wu et al., 2020), the actual sequence ϕ_t tracks this stable equilibrium as $t \to \infty$.

On the slower timescale, we consider the actor update:

$$(\mathbf{w},\mathbf{q})_{t+1} \ = \ (\mathbf{w}, \mathbf{q})_t \ + \ \alpha_{(\mathbf{w},\mathbf{q})}(t)\, \nabla_{(\mathbf{w},\mathbf{q})} \log \pi_{(\mathbf{w},\mathbf{q})_t}(a_t \mid s_t)\, \widehat{A}_t.$$

As ϕ_t converges quickly to $\phi^*(\mathbf{w}, \mathbf{q})$, the advantage estimate $\widehat{A}_t$ converges to $A^{\pi_{(\mathbf{w},\mathbf{q})}}(s_t, a_t)$. Hence, up to diminishing approximation errors, the gradient update for our rule based model is driven from the true policy gradient from the policy gradient theorem. Based on Theorem 4.5, ignoring the small the errors, we have

$$G((\mathbf{w}, \mathbf{q});\ \phi^*(\mathbf{w}, \mathbf{q})) \ = \ \nabla_{wq} J(\mathbf{w}, \mathbf{q}).$$

Putting the fast and slow processes together, we return to the coupled ODE; By the previous steps:

$$F(\phi;\ (\mathbf{w}, \mathbf{q})) = 0 \ \text{ implies } \ \phi = \phi^*, \tag{11}$$

$$G((\mathbf{w}, \mathbf{q});\ \phi^*) \ \approx \ \nabla_{wq} J(\mathbf{w}, \mathbf{q}). \tag{12}$$

Hence, an equilibrium $\big(\phi^*, (\mathbf{w}, \mathbf{q})\big)$ of the ODE occurs precisely, when

$$F(\phi^*; (\mathbf{w}, \mathbf{q})) = 0 \quad \text{and} \quad G((\mathbf{w}, \mathbf{q});\ \phi^*) = 0,$$

which in turn implies

$$\nabla J(\mathbf{w}, \mathbf{q}) = 0, \quad \text{if the advantage estimation is unbiased.}$$

Therefore, the equilibrium corresponds to a stationary point of $J(w, q)$. Under mild conditions (e.g., local convexity/concavity arguments or strict monotonicity), one concludes that the limit points are *local maxima* of $J(w, q)$.

We now invoke the standard *Two-timescale* theorems (Borkar & Meyn, 2000; Wu et al., 2020). then the combined updates converge to an *internally consistent* equilibrium of the ODE. By the structure of the ODE, the equilibrium is a stationary point and *local* optimal of $J(w, q)$. □

E Hybrid Warm Start for Accelerating Convergence

In NSAC, we also adopt a novel hybrid training strategy that incorporates both neural network-based actor and rule-based actor. This hybrid strategy seeks to merge the quick learning attributes of neural networks with the clear and straightforward nature of rule-based systems.

Step 1: We employ a traditional neural network-based actor-critic model to train the system. In this phase, both the actor and the critic are implemented as neural networks, leveraging their ability to approximate complex functions and capture high-dimensional patterns in the data. The model is trained for a certain number of episodes but not until complete convergence. This pre-training phase is designed to establish a preliminary value function estimation that captures essential features of the optimal strategies in a computationally efficient manner.

Step 2: The neural network-based actor is replaced with the rule ensemble actor. This rule-based system is designed to provide greater transparency and interpretability in decision-making. With the rule ensemble actor in place, training continues, utilizing the previously trained neural network critic. The critic assists the new actor in refining its policy through ongoing feedback and value estimation.

E.1 Ablation Study

In our ablation study, we explored how variations in the rule count and the implementation of a warm start influenced our method. We conducted tests in the CartPole-v1 environment under various rule configurations, specifically using 5, 10, 12, 20, 30, 40, and 50 rules per action. Each configuration was tested both with and without a warm start.

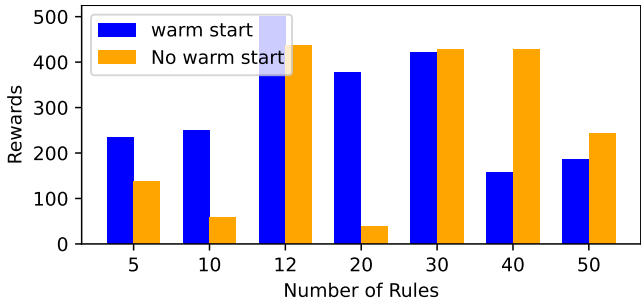

Figure 5: Ablation study on different numbers of rules and warm start.

1. Number of Rules: As depicted in Figure 5, the model configured with 12 rules per action and a warm start yields the highest reward. This outcome suggests that having 12 rules per action provides the model with sufficient flexibility to effectively capture the essential dynamics of the environment without being overly simplistic. Employing fewer than 10 rules, such as 5, may not offer adequate coverage to manage the environment's complexity, resulting in inferior performance. Conversely, a larger number of rules may lead the model to overfit the training data, picking up on noise or irrelevant patterns and diminishing its generalizability to new contexts. The findings from this ablation study highlight a critical balance between the number of rules and overall model performance. They demonstrate that merely increasing the number of rules does not invariably improve performance, as an excess can lead to complexity and overfitting, whereas too few can restrict the model's performance.

2. Warm Start: When the number of rules is small, the model's representational capability is limited, so the initial conditions (e.g., the warm start) become more critical. A warm start can guide the model toward better solutions early on, helping it learn an effective policy faster and avoid getting stuck in poor local optima. In contrast, with a larger rule set, the model has greater capacity to explore various configurations. In such cases, relying on an external initialization can sometimes constrain exploration, preventing the model from fully leveraging its increased flexibility. As a result, the model without a warm start may discover a better configuration on its own when there are many rules to learn from.

F Continuous Environments

Continuous environments differ fundamentally from the perspective of the theoretical framework we propose. In this work, theoretical analysis is restricted to discrete action spaces, as our method enables us to establish formal convergence guarantees.

In order to guarantee the convergence of our proposed method, we restrict our analysis to discrete action spaces. The convergence proof relies on several technical assumptions—such as bounded gradients, Lipschitz continuity, and stable critic updates—that are typically satisfied in discrete action spaces, but are difficult to guarantee in continuous settings, particularly for actor–critic methods ([3] and [33] in submitted manuscript). Discrete policies (e.g., softmax) yield smooth and bounded log-policy gradients, which facilitate stable actor updates and tractable Bellman backups using finite sums. These same conditions are also required for the convergence of the rule-based function class used in OGB. As a gradient-boosting-based algorithm, OGB requires the loss function to be Lipschitz continuous, which means that the gradients are bounded. According to Theorem 2.4, 2.8 and 2.9 in Shalev-Shwartz et al. (2010) (cited in original paper as [28]), Lipschitz continuity is a necessary condition for the learned models to converge to a theoretically optimal model within a certain number of iterations for (fully corrective) boosting methods and the rule replacement steps.

In contrast, continuous action spaces present challenges, such as unbounded gradients (e.g., the policy gradient can become unbounded as the standard deviation in Gaussian policies), integration-based Bellman targets, and higher variance in gradient estimates. These factors violate the core assumptions underpinning both the two-timescale stochastic approximation framework and the rule ensemble model used in our convergence analysis.

G Related Work

Ref	Work (short)	Category	Interp. at scale	P/Pt/E	Performance
[9,13]	Tree-based batch RL	Tree policy (native)	Not interp.(large trees)	N/N/Y	Strong on S/M; degrades on L/complex
[31]	Tree RL for DTRs	Tree policy (native)	Not interp.(multi-stage)	N/N/Y	Hard to scale beyond structured domains
[1]	Policy extraction	Tree policy (extracted)	Often not interp. (size balloons)	N/Y/N	Tracks teacher; small typical drop
[25]	Conservative Q-Improvement	Tree policy (native)	Not interp.(large trees)	N/N/Y	Strong on S/M; degrades on L/complex
[29]	Differentiable decision trees	Tree policy (diff.)	Not interp.(math notation)	N/N/Y	Solid on modest tasks; mixed scaling
[8]	Cascading Decision Trees	Tree policy (native)	Not interpretable at scale	N/N/Y	Good early; plateaus with complexity
[14]	Policy Tree(distill.)	Tree policy (distilled)	Often not interpretable at scale	N/Y/N	Tracks teacher; bigger drop for small trees
[5]	Soft DT distillation	Tree policy (distilled)	Often not interpretable at scale	N/Y/N	Approximates teacher; mild–moderate drop
[18]	Linear Model U-Trees	Tree policy (distilled)	Not interp.(math notation)	N/Y/N(only)	Good local fidelity; may trail overall
[12]	SRL with commonsense	Symbolic RL (predefined)	Interpretable (symbolic rules)	Y/N/Y	Strong when priors fit; brittle if misspecified
[19]	SDRL (symbolic planning)	Symbolic RL (predefined)	Interpretable (modules)	Y/N/Y	Often strong & sample-efficient; planner-dependent
[16]	Symbolic plans as instr.	Symbolic RL (predefined)	Interpretable (plans)	Y/N/Y	Good when plans align; limited otherwise
[17]	Discovering symb. policies	Symbolic policy (from NN)	Not interp.(math notation)	N/Y/N	Near-teacher on seen tasks; drops under shift
[15]	GP-based symbolic rules	Symbolic policy (direct)	Not interp.(math notation)	N/N/Y	Competitive on simpler control; search limits scale
[32]	Programmatic RL (PIRL)	Program synthesis policy	Not interp.(math notation)	N/N/Y	Lags in high-dimensional
Ours	NSAC	Symbolic RL	Interpretable(symbolic rules)	N/N/Y	Often strong & sample-efficient

Table 2: Compact comparison of policy representations and learning setups.

We summarise representative interpretable RL approaches across tree-based, symbolic, and programmatic policy classes. *Interp. at scale* highlights whether interpretability persists as problem size/complexity grows. *P/Pt/E* abbreviates *Predefined knowledge? / Post-hoc from pretrained? / Learn directly from environment?* (Y/N). *Performance* sketches typical empirical behaviour. Overall, native tree policies often face scalability–interpretability trade-offs, post-hoc distilled trees track teachers but lose fidelity when heavily pruned, symbolic methods offer strong transparency and sample efficiency when priors/plans match the domain, and programmatic policies remain challenging in high-dimensional settings.

H BENCHMARK SETTING

We recognize that certain algorithms might perform better with changes to the environment (e.g., adjusting the number of parallel environments or modifying rewards). Still, finding a single modification that consistently benefits all tested algorithms remains challenging. Therefore, we rely on the most basic version of each environment to maintain consistency across all methods. Additionally, it is important to note that the complexity of our model is designed to balance comprehensibility with the cognitive effort needed to understand all of the rules involved. Therefore, in our paper, we deliberately selected 12 rules per action model, which helps ensure the interpretability of our proposed method.

All experiments in this paper are conducted on a computer with processor "3.1GHz 6-Core Intel Core i5" and a memory of "72GB 2133 MHz DDR4".

I ENVIRONMENT DESCRIPTIONS

I.1 CARTPOLE-V1

The *CartPole-v1* environment involves a pole attached by an un-actuated joint to a cart, which moves along a frictionless track. The system is controlled by applying a force of $+1$ or -1 to the cart. The pole starts upright, and the goal is to prevent it from falling over. A reward of $+1$ is provided for every timestep that the pole remains upright. The episode ends when the pole is more than 15 degrees from vertical, or the cart moves more than 2.4 units from the center.

I.2 MOUNTAINCAR-V0

In the *MountainCar-v0* environment, a car is positioned between two hills and the objective is to drive up the right-hand hill, which the car cannot accomplish without first backing up the left hill to gain momentum. The reward is -1 for each time step, until the car reaches the goal, encouraging the car to reach the goal as quickly as possible.

I.3 ACROBOT-V1

The *Acrobot-v1* environment consists of a two-link, two-joint robot, or "acrobot," which is actuated only at the joint between the two links. The objective is to swing the end of the lower link up to a given height by applying torques to the actuated joint. The reward is -1 for each timestep until the goal is reached. The environment is considered solved when the end of the lower link swings above the specified height.

I.4 BLACKJACK-V0

The *Blackjack-v0* environment simulates the game of blackjack, where the objective is to obtain cards whose sum is as close to 21 as possible without going over. The agent plays against a dealer, and can request additional cards (*hit*) or stop (*stick*). The reward is $+1$ for winning, -1 for losing, and 0 for a draw. The game follows typical Blackjack rules as found in casinos.

I.5 POSTMAN

In this custom environment, the agent acts as a postman, tasked with picking up and delivering items at different locations within a grid. The agent must plan efficient routes for picking up and dropping off items, navigating larger grids in the environments.

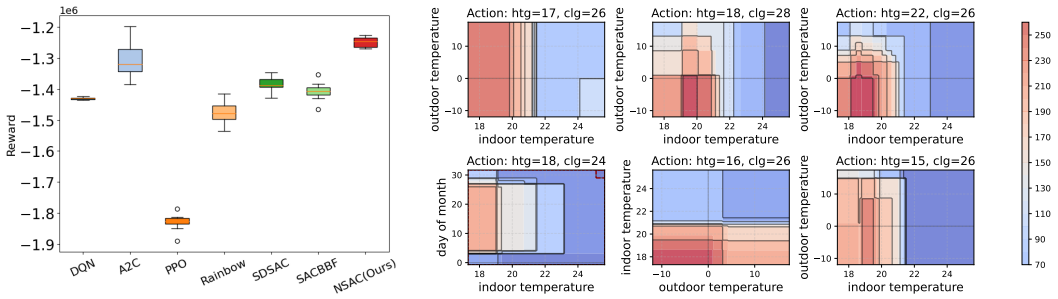

(a) Performance (b) Visualization of the Rules

Figure 6: Comparing the Performance of NSAC with Baseline Methods and Visualize the rules.

J RULES VISUALIZATION FOR HVAC CONTROL WITH SINERGYM

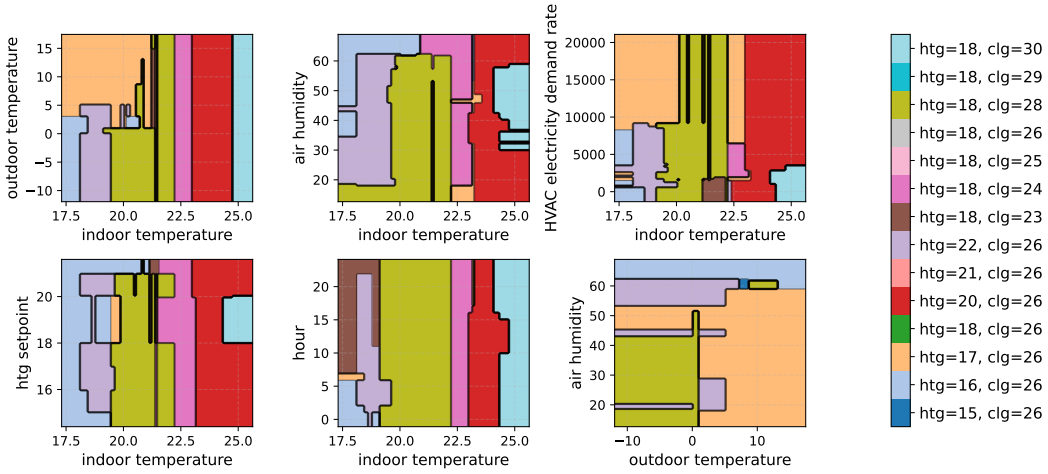

Figure 7: Visualization of action selection for NSAC.

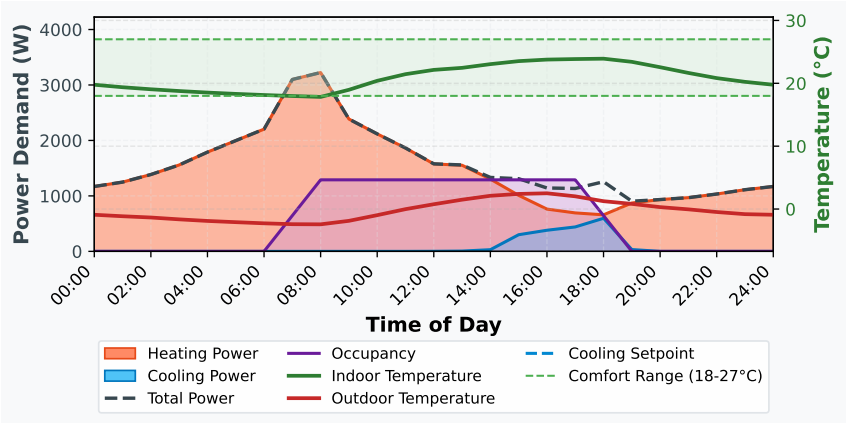

Figure 8: Average performance of our proposed algorithm.

Typical rules for HVAC control with sinergym:

Action htg=16, clg=26:

+50.5500 if $-11.7075 \leq$ outdoor_temperature ≤ 15.0 & htg_setpoint ≤ 20.0 & air_temperature ≤ 20.8431
+42.3222 if hour ≤ 6.0 & $-9.5 \leq$ outdoor_temperature ≤ 4.3200 & air_temperature ≤ 21.1095
+33.7433 if hour ≤ 6.0 & outdoor_temperature ≤ 3.0 & HVAC_electricity_demand_rate ≥ 3524.0383
+30.0530 if air_temperature ≤ 19.4323 & HVAC_electricity_demand_rate ≥ 3492.0372
+23.8401 if hour ≤ 6.0 & outdoor_temperature ≤ -6.0 & HVAC_electricity_demand_rate ≥ 1836.0156
+19.5165 if outdoor_temperature ≤ -5.0 & air_temperature ≤ 20.8367 & air_humidity ≥ 34.4557
+19.3194 if outdoor_temperature ≤ 4.3200 & clg_setpoint ≤ 26.0 & air_temperature ≤ 20.7468 & air_humidity ≥ 44.9061 & HVAC_electricity_demand_rate ≤ 8328.7136
+17.1997 if outdoor_temperature ≤ -6.0 & air_temperature ≤ 20.6569 & air_humidity ≥ 34.4701
+12.2539 if outdoor_temperature ≤ 1.1000 & air_temperature ≤ 19.8760 & air_humidity ≥ 48.4554 & HVAC_electricity_demand_rate ≥ 2194.6457
+10.1033 if day_of_month ≤ 16.0 & outdoor_temperature ≤ -9.5 & air_temperature ≤ 21.4822
+9.9095 if outdoor_temperature ≤ -1.2000 & clg_setpoint ≤ 28.0 & air_temperature ≤ 18.6297 & $20.1259 \leq$ air_humidity ≤ 57.8947
+6.5348 if hour ≤ 5.0 & outdoor_temperature ≤ -6.2000 & air_humidity ≥ 46.6687 & HVAC_electricity_demand_rate ≤ 6047.4648

Action htg=18, clg=26:

+52.4710 if outdoor_temperature ≤ 2.0 & htg_setpoint ≥ 18.0 & air_temperature ≥ 24.6918 & $36.4788 \leq$ air_humidity ≤ 59.9498 & $655.1863 \leq$ HVAC_electricity_demand_rate ≤ 3286.0521
+31.8345 if $-7.3000 \leq$ outdoor_temperature ≤ -2.4800 & clg_setpoint ≥ 28.0 & air_temperature ≥ 22.7824 & air_humidity ≤ 53.0045 & HVAC_electricity_demand_rate ≤ 2804.0908
+25.6196 if day_of_month ≤ 23.0 & hour ≥ 21.0 & htg_setpoint ≥ 18.0 & air_temperature ≤ 21.2843 & $22.2264 \leq$ air_humidity ≤ 57.4836 & HVAC_electricity_demand_rate ≤ 4727.3044
+14.6693 if hour ≤ 16.0 & clg_setpoint ≥ 28.0 & $24.3635 \leq$ air_temperature ≤ 25.3421 & air_humidity ≤ 43.6038 & $1974.6005 \leq$ HVAC_electricity_demand_rate ≤ 2847.7105
+12.8951 if day_of_month ≥ 17.0 & $1.0 \leq$ hour ≤ 5.0 & htg_setpoint ≤ 16.0 & air_temperature ≤ 19.6280 & HVAC_electricity_demand_rate ≥ 728.1273
+6.6281 if $14.0 \leq$ hour ≤ 15.0 & outdoor_temperature ≤ -2.4800 & $24.1909 \leq$ air_temperature ≤ 25.1225 & air_humidity ≤ 44.0097 & HVAC_electricity_demand_rate ≤ 2856.4850
+3.6962 if outdoor_temperature ≤ -2.4800 & air_temperature ≥ 25.9993
+2.2511 if hour ≥ 18.0 & $-5.0 \leq$ outdoor_temperature ≤ -2.4800 & air_temperature ≥ 22.3801 & air_humidity ≤ 52.5242 & $1164.7935 \leq$ HVAC_electricity_demand_rate ≤ 1443.5973
+1.7191 if $-7.3000 \leq$ outdoor_temperature ≤ -3.0 & clg_setpoint ≥ 30.0 & air_humidity ≤ 52.1981 & $1411.8365 \leq$ HVAC_electricity_demand_rate ≤ 2783.3056
+1.6791 if $5.0 \leq$ day_of_month ≤ 28.0 & $-3.4000 \leq$ outdoor_temperature ≤ 6.6000 & $22.4682 \leq$ air_temperature ≤ 23.2356 & HVAC_electricity_demand_rate ≤ 1559.4128

Action htg=18, clg=25:

+76.0682 if month ≤ 2.0 & day_of_month ≤ 29.0 & $-2.4800 \leq$ outdoor_temperature ≤ 15.0 & htg_setpoint ≤ 21.0 & air_temperature ≤ 20.4542

+35.7797 if month ≤ 2.0 & day_of_month ≤ 28.0 & outdoor_temperature ≤ 15.0 & air_temperature ≤ 20.4547 & HVAC_electricity_demand_rate ≤ 888.4346

+19.5429 if hour ≤ 17.0 & outdoor_temperature ≤ 4.3200 & air_temperature ≥ 21.3982 & air_humidity ≥ 22.1544 & HVAC_electricity_demand_rate ≥ 3353.0663

+11.0059 if outdoor_temperature ≤ -7.3000 & air_temperature ≥ 23.0022 & HVAC_electricity_demand_rate ≥ 3343.0970

+10.4447 if month ≤ 1.0 & outdoor_temperature ≤ 0.0 & air_temperature ≥ 22.3607 & air_humidity ≥ 35.8469 & HVAC_electricity_demand_rate ≥ 3237.7531

+9.2884 if day_of_month ≤ 28.0 & $-2.4800 \leq$ outdoor_temperature ≤ 15.0 & clg_setpoint ≤ 25.0 & air_temperature ≤ 20.4644

+8.4585 if hour ≤ 16.0 & air_temperature ≥ 23.5872 & HVAC_electricity_demand_rate ≥ 3378.0424

+7.6878 if $2.0 \leq$ day_of_month ≤ 8.0 & hour ≤ 15.0 & outdoor_temperature ≤ -6.7000 & air_temperature ≥ 22.9565 & HVAC_electricity_demand_rate ≤ 5120.2045

+6.0944 if hour ≤ 16.0 & outdoor_temperature ≤ -9.5 & air_temperature ≥ 22.3765

+6.0912 if $-2.4800 \leq$ outdoor_temperature ≤ 1.0 & clg_setpoint ≤ 29.0 & air_temperature ≤ 18.5048 & $28.1472 \leq$ air_humidity ≤ 57.5569

+4.1747 if air_temperature ≥ 25.1225 & HVAC_electricity_demand_rate ≥ 4135.6304

+2.7032 if $2.0 \leq$ day_of_month ≤ 29.0 & hour ≥ 1.0 & $-11.7075 \leq$ outdoor_temperature ≤ -5.6000 & $18.0977 \leq$ air_temperature ≤ 24.9366 & $4026.8635 \leq$ HVAC_electricity_demand_rate ≤ 7054.0210

Action htg=18, clg=28:

+47.6207 if outdoor_temperature ≤ 1.1000 & air_temperature ≤ 21.3847

+42.5021 if month ≤ 2.0 & outdoor_temperature ≤ 13.0150 & clg_setpoint ≤ 29.0 & air_temperature ≤ 20.8932 & HVAC_electricity_demand_rate ≤ 9236.5036

+37.5818 if month ≤ 2.0 & htg_setpoint ≤ 21.0 & $19.0381 \leq$ air_temperature ≤ 22.2181 & air_humidity ≤ 61.5915

+37.5560 if month ≤ 2.0 & htg_setpoint ≤ 21.0 & $19.0971 \leq$ air_temperature ≤ 24.1215 & air_humidity ≤ 62.4223

+26.1161 if outdoor_temperature ≤ -3.4000 & $17.0 \leq$ htg_setpoint ≤ 18.0 & air_temperature ≤ 21.6418 & HVAC_electricity_demand_rate ≥ 1616.5198

+25.3651 if month ≤ 2.0 & hour ≤ 6.0 & outdoor_temperature ≤ 8.8000 & air_temperature ≤ 21.0920 & air_humidity ≤ 51.7392

+21.4283 if hour ≤ 6.0 & outdoor_temperature ≤ -2.0 & htg_setpoint ≤ 18.0 & air_temperature ≤ 20.0191 & HVAC_electricity_demand_rate ≥ 1266.1656

+19.3831 if air_temperature ≤ 19.0718

+18.9771 if clg_setpoint ≥ 28.0 & air_temperature ≤ 22.6279 & $3313.9887 \leq$ HVAC_electricity_demand_rate ≤ 9094.2658

+15.9370 if outdoor_temperature ≤ 1.0 & htg_setpoint ≤ 20.0 & air_temperature ≤ 21.1680 & air_humidity ≥ 46.0692 & HVAC_electricity_demand_rate ≥ 3766.4288

+11.4827 if outdoor_temperature ≤ 1.1000 & air_temperature ≤ 18.9835 & $2059.7858 \leq$ HVAC_electricity_demand_rate ≤ 8526.6964

+11.1224 if $3.0 \leq$ day_of_month ≤ 28.0 & hour ≥ 22.0 & outdoor_temperature ≤ -1.0 & htg_setpoint ≤ 18.0 & $20.5696 \leq$ air_humidity ≤ 57.0262 & HVAC_electricity_demand_rate ≥ 2007.6986

K RULES VISUALIZATION FOR BLACKJACK-V1

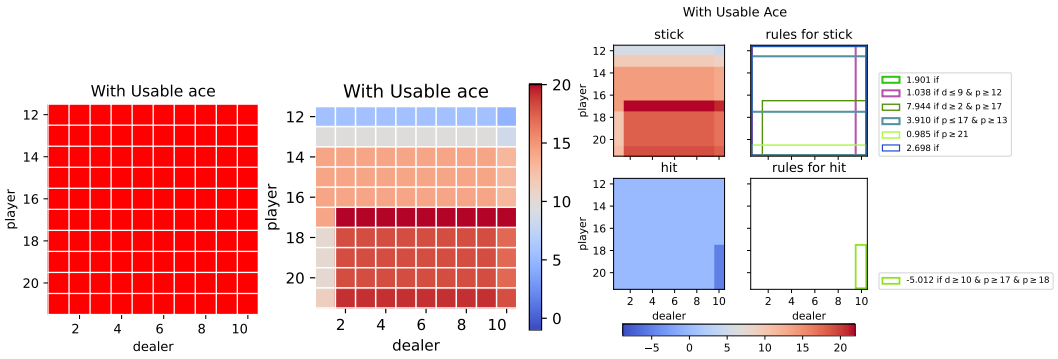

Figure 9: Visualization for action, value and rules for Blackjack with Ace.

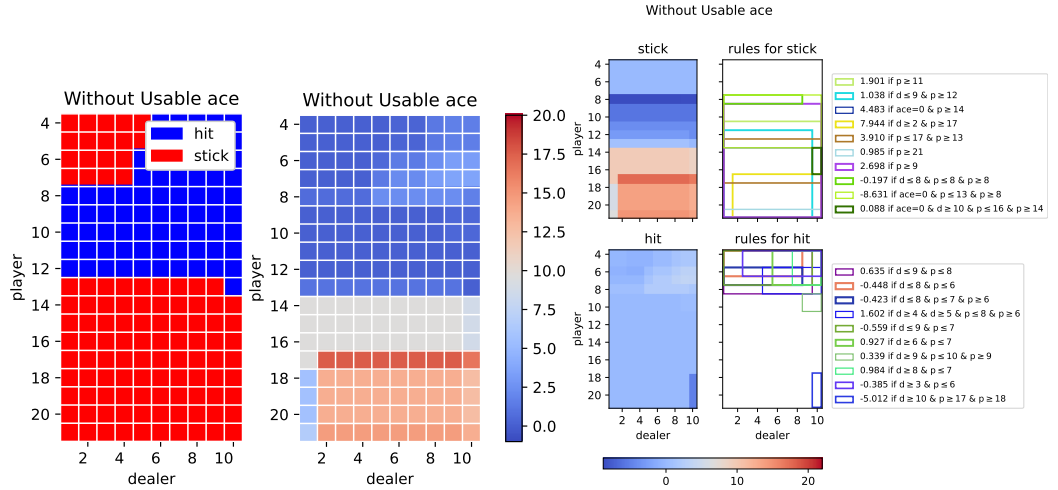

Figure 10: Visualization for action, value and rules for Blackjack with no Ace.

Action 0 (Stick):

$$
\begin{aligned}
&+1.9012 \quad \text{if } p \geq 11 \\
&+1.0376 \quad \text{if } d \leq 9 \text{ and } p \geq 12 \\
&+4.4833 \quad \text{if ace} \geq 1 \text{ and } p \geq 14 \\
&+7.9438 \quad \text{if } d \geq 2 \text{ and } p \geq 17 \\
&+3.9105 \quad \text{if } p \leq 17 \text{ and } p \geq 13 \\
&+0.9851 \quad \text{if } p \geq 21 \\
&+2.6981 \quad \text{if } p \geq 9 \\
&-0.1967 \quad \text{if } d \leq 8 \text{ and } d \leq 9 \text{ and } p \leq 8 \text{ and } p \geq 8 \\
&-8.6313 \quad \text{if ace} \leq 0 \text{ and } p \leq 13 \text{ and } p \geq 8 \\
&+0.0882 \quad \text{if ace} \leq 0 \text{ and } d \geq 10 \text{ and } p \leq 16 \text{ and } p \geq 14
\end{aligned}
$$

Action 1 (Hit):

$$
\begin{array}{ll}
+0.6347 & \text{if } d \leq 9 \text{ and } p \leq 8 \\
-0.4481 & \text{if } d \leq 8 \text{ and } p \leq 6 \\
-0.4231 & \text{if } d \leq 8 \text{ and } p \leq 7 \text{ and } p \geq 6 \\
+1.6016 & \text{if } d \geq 4 \text{ and } d \geq 5 \text{ and } p \leq 8 \text{ and } p \geq 6 \\
-0.5585 & \text{if } d \leq 9 \text{ and } p \leq 7 \\
+0.9266 & \text{if } d \geq 6 \text{ and } p \leq 7 \\
+0.3394 & \text{if } d \geq 9 \text{ and } p \leq 10 \text{ and } p \geq 9 \\
+0.9844 & \text{if } d \geq 8 \text{ and } p \leq 7 \\
-0.3849 & \text{if } d \geq 3 \text{ and } p \leq 6 \\
-5.0124 & \text{if } d \geq 10 \text{ and } p \geq 17 \text{ and } p \geq 18
\end{array}
$$

L MountainCar Rules

Action Left:

$$
\begin{array}{ll}
+25.3111 & \text{if } v \leq -0.0006471572560258208 \\
-10.5678 & \text{if } p \leq -0.5023447513580322 \\
+53.8697 & \text{if True} \\
+51.0351 & \text{if } v \leq -0.004265955928713083 \\
-14.5140 & \text{if } p \geq -0.5813989758491516 \text{ and } v \leq 0.006803702469915152 \\
 & \text{and } v \geq -0.0008947865571826689 \\
-11.6162 & \text{if } p \leq -0.41075775027275085 \text{ and } v \leq -0.000661600707098839 \\
+17.6882 & \text{if } v \geq -1.5593287753289978 \times 10^{-5} \\
+16.4293 & \text{if } p \leq -0.25240878462791444 \text{ and } p \geq -0.6275408387184143 \\
 & \text{and } v \leq 0.01510303020477297 \text{ and } v \geq -0.01191 \\
-17.9516 & \text{if } p \leq -0.4901819765567779 \text{ and } p \geq -0.615831172466278 \\
 & \text{and } v \leq 0.00759 \text{ and } v \geq -0.004150 \text{ and } v \geq 0.00126822 \\
+21.4738 & \text{if } v \leq 0.00040989847620949166 \\
-2.3676 & \text{if } p \geq -0.5437554597854615 \text{ and } v \leq 0.0016861518379300846 \\
 & \text{and } v \geq -0.0034104006830602885 \\
+1.2316 & \text{if } p \leq -0.1402401 \text{ and } p \geq -0.4494079709053038 \\
 & \text{and } v \leq 0.023414026945829402 \text{ and } v \geq -0.01632060520350933
\end{array}
$$

No Action:

$$
\begin{aligned}
-19.7248 \quad & \text{if } p \geq -0.5101138830184937 \text{ and } v \leq 0.006803702469915152 \\
& \text{and } v \geq -0.005573090445250273 \\
-13.4848 \quad & \text{if } v \geq 0.0007145821116864693 \\
+24.2199 \quad & \text{if } p \geq -0.4848527312278747 \text{ and } v \leq 0.00018940809495689726 \\
& \text{and } v \geq -0.009227151423692702 \\
-23.3706 \quad & \text{if } v \leq 0.003292182506993414 \\
-6.6878 \quad & \text{if } v \leq -9.685811237431741 \times 10^{-5} \\
+24.7429 \quad & \text{if } p \leq -0.4022643387317657 \\
& \text{and } v \leq 0.00020952874911017827 \\
-26.5154 \quad & \text{if } p \geq -0.6311534523963929 \text{ and } v \leq 0.006872396916151048 \\
& \text{and } v \geq -0.006245836243033409 \\
-8.7515 \quad & \text{if } p \geq -0.39260063171386717 \text{ and } v \geq 0.0019062188919633629 \\
+0.7214 \quad & \text{if } v \leq -0.006146392878144977 \\
-0.9839 \quad & \text{if True} \\
+6.8736 \quad & \text{if } p \geq -0.5437554597854615 \text{ and } v \leq 0.0038646903820335875 \\
+1.0000 \quad & \text{if } v \geq -0.0010096890269778618
\end{aligned}
$$

Action Right:

$$
\begin{aligned}
+26.2150 \quad & \text{if } p \leq -0.5101138830184937 \text{ and } v \leq 0.006803702469915152 \\
+6.3636 \quad & \text{if } p \geq -0.4848527312278747 \text{ and } v \geq -0.009227151423692702 \\
+6.1251 \quad & \text{if } p \geq -0.4855665504932403 \text{ and } v \geq 0.003292182506993414 \\
+24.0837 \quad & \text{if True} \\
+27.5176 \quad & \text{if } p \leq -0.4022643387317657 \text{ and } v \leq 0.0012711382005363714 \\
+21.3072 \quad & \text{if } v \geq 0.0007119119516573855 \\
+18.6883 \quad & \text{if } v \leq -0.0005520289996638883 \\
+19.7662 \quad & \text{if } v \geq 0.0004626010428182804 \\
+21.3412 \quad & \text{if } p \leq -0.6329279899597166 \\
+11.7750 \quad & \text{if } p \geq -0.5767600297927856 \text{ and } v \geq 0.0012682238826528204 \\
+16.5113 \quad & \text{if } v \geq 0.00040989847620949166 \\
+1.3610 \quad & \text{if } p \leq -0.4494079709053038 \text{ and } p \geq -0.8744302272796631 \text{ and } v \leq 0.023414026945829402
\end{aligned}
$$

M Explanation of Cart-Pole Rules

The CartPole environment consists of a pole mounted on a cart that moves along a track. The objective is to balance the pole upright by controlling the cart's movement left or right. The state space includes the cart's position(p), velocity(v), pole angle(θ), and angular velocity($\dot{\theta}$), while the action space includes applying force to move the cart in either direction. Figure 11 is the visualization of our actor's rule regarding the position and velocity. Please refer to Appendix N for all the resulted rules.

Here we will use a typical state in the Cart-Pole game, where the optimal action is to move the cart to the right, characterized by the parameters $p = -0.05, v = 0.1, \theta = 0.05$ and $\dot{\theta} = 0.3$, as an example to illustrate the decision-making process for our proposed method. In this scenario, pushing right reduces the pole's angular velocity, helping stabilize the pole by balancing the torque induced by the tilt. In our model, three rules become active when considering a leftward action; each rule incurs a negative score because the pole's angle is positive, decisively discouraging a left move. In contrast, the overall score for moving right is 2.3, notably higher than that for moving left. Although the cart's slight leftward position imposes a small penalty, the pole's rightward angular velocity plays a critical role: one rule alone contributes +19.8 to the total, effectively countering any negative effects from the

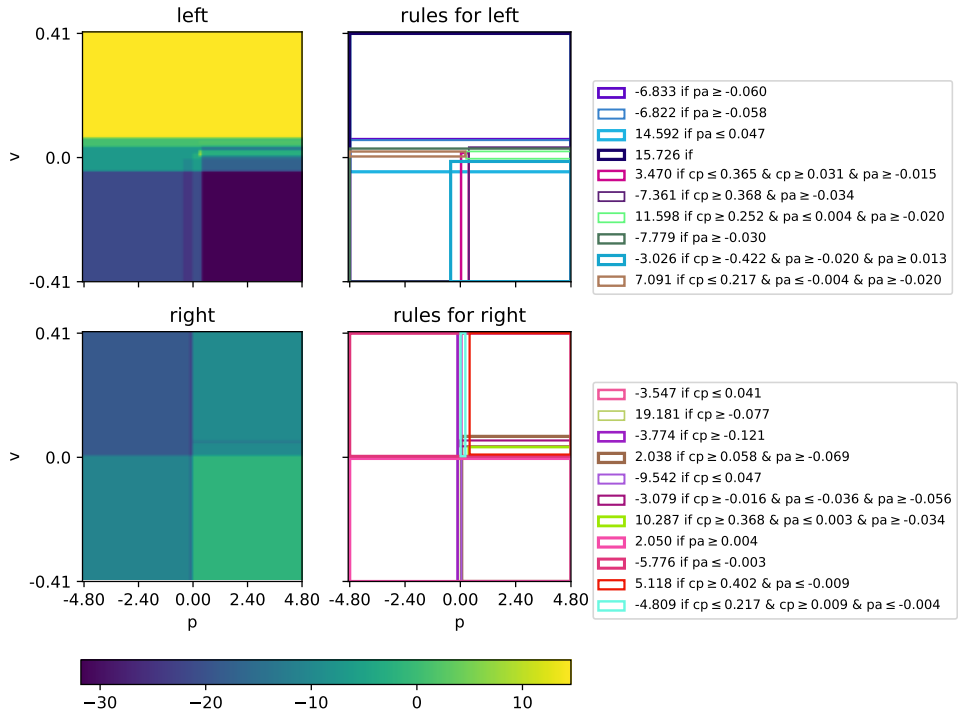

Figure 11: Visual representation of the rules for CartPole involving position and velocity.

other rules. Consequently, given the pole's rightward tilt and velocity, the agent's optimal choice is to push right, thereby maintaining stability and preventing undesirable outcomes.

N CartPole Rules

Left:

-6.83310	if pa ≥ -0.06048
-6.82240	if pa ≥ -0.05751
$+14.59180$	if pa ≤ 0.04701 and pav ≤ 0.26781
$+15.72630$	if pav ≤ -0.52576
$+3.47030$	if cp ≤ 0.36470 and cp ≥ 0.03103 and cv ≤ 0.20766 and cv ≥ -0.00962 and pa ≥ -0.01513 and pav ≤ 0.28779 and pav ≥ -0.05232
$+0.88280$	if cp ≥ 0.24231 and cv ≥ -0.40319 and pa ≤ -0.03636 and pa ≥ -0.05565
-7.36080	if cp ≥ 0.36775 and cv ≥ -0.00425 and pa ≥ -0.03416 and pav ≤ 0.12249
$+11.59770$	if cp ≥ 0.25174 and pa ≤ 0.00381 and pa ≥ -0.02022 and pav ≤ 0.11855 and pav ≥ -0.37647
-7.77910	if pa ≥ -0.02969
-0.86900	if cp ≤ 0.16311 and cp ≤ 0.30448 and cp ≥ -0.11618 and cv ≤ -0.01313 and cv ≤ 0.17905 and pa ≤ 0.03930 and pa ≥ -0.02479 and pav ≤ 0.14835
-3.02560	if cp ≥ -0.42154 and cv ≤ 0.32329 and cv ≥ -0.01879 and pa ≥ -0.02018 and pa ≥ 0.01293 and pav ≤ 0.13896 and pav ≥ -0.01362
$+7.09090$	if cp ≤ 0.21659 and cv ≤ 0.21317 and cv ≥ -0.00898 and pa ≤ -0.00355 and pa ≥ -0.01990 and pav ≤ -0.29080

Right:

-3.54700	if cp ≤ 0.04146
$+19.18060$	if cp ≥ -0.07721 and pav ≥ 0.20059
-3.77380	if cp ≥ -0.12061
$+2.03760$	if cp ≥ 0.05832 and cv ≤ 0.06116 and pa ≥ -0.06911 and pav ≤ -0.05532
-9.54210	if cp ≤ 0.04726
-3.07880	if cp ≥ -0.01648 and cv ≤ 0.16053 and cv ≥ -0.19434 and pa ≤ -0.03636 and pa ≥ -0.05565
$+10.28650$	if cp ≥ 0.36775 and cv ≥ -0.00425 and cv ≥ 0.20400 and pa ≤ 0.00317 and pa ≥ -0.03416 and pav ≤ 0.12249 and pav ≥ -0.37842
$+2.04960$	if cv ≥ -0.34930 and pa ≥ 0.00381 and pav ≤ 0.11855
-5.77560	if cv ≥ -0.36800 and pa ≤ -0.00339
$+5.11750$	if cp ≥ 0.40156 and cv ≤ 0.39100 and pa ≤ -0.00914 and pav ≤ -0.33129
$+0.00510$	if cp ≥ 0.02529 and cv ≥ -0.01879 and pa ≤ 0.03998 and pa ≥ 0.01293 and pav ≥ 0.13896
-4.80880	if cp ≤ 0.21659 and cp ≥ 0.00944 and cv ≤ -0.28634 and pa ≤ -0.00355 and pav ≤ 0.30114 and pav ≥ -0.01324

O ACROBOT RULES

0:

$+8.7846$	if $w_1 \geq -0.09082$ and $w_2 \leq 0.22991$
$+9.3353$	if $\cos(\theta_2) \geq 0.89409$
$+10.4909$	if $\sin(\theta_2) \leq 0.44980$
$+8.2458$	if $\sin(\theta_2) \leq 0.37771$ and $w_1 \geq -0.12610$ and $w_2 \leq 0.15699$
$+11.6541$	if True
$+6.8474$	if $\sin(\theta_1) \leq 0.24220$ and $w_2 \leq 0.04877$
$+1.2850$	if $\cos(\theta_2) \geq 0.99115$ and $\sin(\theta_1) \leq -0.01332$
$+1.7239$	if $\sin(\theta_1) \leq -0.01472$ and $w_2 \leq 0.02869$
$+3.5813$	if $\cos(\theta 1) \geq 0.88816$ and $\sin(\theta_1) \geq -0.28723$ and $w_1 \leq 0.77240$
$+1.3335$	if $\cos(\theta_1) \geq 0.48252$ and $w_1 \leq 1.78991$ and $w_1 \geq -1.70488$
$+1.0000$	if $\cos(\theta_2) \leq 0.95137$ and $\sin(\theta_1) \geq 0.01719$

1:

-3.0189 if $\cos(\theta_2) \leq 0.99319$
-3.3464 if $\cos(\theta_1) \leq 0.99048$ and $w_2 \leq 0.12677$
-8.6917 if $\cos(\theta_1) \geq 0.81787$ and $w_1 \leq 0.92265$
-5.4697 if True
-9.3263 if $w_1 \leq 0.21755$ and $w_2 \geq -0.10354$
-5.5746 if $\sin(\theta_2) \leq 0.37771$ and $w_1 \leq 1.28679$ and $w_2 \geq 0.15699$
$+5.4709$ if $\sin(\theta_1) \geq -0.26647$ and $\sin(\theta_2) \leq 0.44500$ and $w_1 \geq -1.07104$ and $w_2 \leq 0.04877$
-8.2010 if $\sin(\theta_1) \leq 0.04400$
$+1.5784$ if $\cos(\theta_1) \geq 0.99341$
-9.7897 if $\sin(\theta_1) \leq 0.15513$ and $\sin(\theta_1) \geq -0.70608$ and $\sin(\theta_2) \geq -0.17949$ and $w_1 \leq 1.78991$ and $w_1 \geq -1.70488$
-1.2848 if $\cos(\theta_1) \geq 0.99674$
$+1.0000$ if $\cos(\theta_2) \leq 0.99350$ and $\sin(\theta_1) \leq -0.21224$ and $w_1 \geq 0.11238$ and $w_2 \leq -0.22888$

2:

$+3.5980$ if $\cos(\theta_1) \geq 0.99689$
$+2.5385$ if $\cos(\theta_1) \geq 0.99048$
$+16.7525$ if True
-3.7130 if $\cos(\theta_1) \leq 0.99999$ and $\sin(\theta_2) \leq -0.01789$
-1.9920 if $\sin(\theta_2) \leq -0.00190$
$+12.0937$ if $w_1 \leq -0.02180$ and $w_2 \geq 0.04994$
$+9.6534$ if $w_2 \geq 0.04994$
$+1.1957$ if $\cos(\theta_2) \geq 0.24062$ and $w_1 \geq -0.32756$ and $w_2 \leq 1.64803$
-3.6820 if $w_1 \geq -0.12540$
$+15.8530$ if $\cos(\theta_1) \geq 0.88816$ and $w_2 \geq -0.41702$
$+10.0707$ if $\cos(\theta_1) \leq 0.99674$ and $\cos(\theta_2) \geq 0.92457$
$+1.6685$ if $\cos(\theta_2) \leq 0.99350$ and $\sin(\theta_1) \leq -0.21224$ and $w_1 \geq 0.11238$ and $w_2 \leq -0.22888$

P STATEMENT ON LLM USAGE

Large language models (LLMs), such as ChatGPT, were used solely for editorial assistance in this work. Their role was limited to improving grammar, rephrasing sentences, and enhancing clarity and readability of the authors' original text. No LLM was used to generate original scientific content, analysis, or results. The authors take full responsibility for the integrity and validity of the work presented.